Aalto University

School of Chemical Technology
Department of Biotechnology and Chemical Technology
Chemical Engineering Research Group

Moshood Abdulwahab

MODELLING OF IONIC LIQUIDS' THERMAL SEPARATION AND RECYCLING IN BIOMASS FRACTIONATION

Master's thesis for the degree of Master of Science in Technology

submitted for inspection,

Espoo, 28th August, 2013.

Supervisor: Professor Ville Alopaeus
Instructor: D.Sc. (Tech.) Kaj Jakobsson

Aalto University
School of Chemical
Technology

Aalto University, P.O. BOX 11000, 00076 AALTO
www.aalto.fi

Abstract of master's thesis

Author	Moshood Abdulwahab
Title of thesis	Modelling of ionic liquids' thermal separation and recycling in biomass fractionation
Department	Biotechnology and Chemical Technology
Professorship	Chemical Engineering
Code of professorship	KE-42
Thesis supervisor	Professor Ville Alopaeus
Thesis advisor(s) / Thesis examiner(s)	D.Sc. (Tech.) Kaj Jakobsson
Date	28.08.2013
Number of pages	63 + Appendices
Language	English

Abstract

Ionic liquids (ILs) as a fractionating agent have shown promising potentials to offer greener and safer technology with regards to making biomass as feedstock for energy and biochemicals production. Several laboratory-scale experiments have reported fractionating biomass with different types of ILs alongside the procedure for recovering the dissolved biomass fractions and the spent IL. For the sake of economical industrial practice, the most promising type of IL with regards to separability and recyclability in biomass fractionation process must be identified.

In response to this research gap, this thesis seeks to investigate the most promising type of IL via modelling of their thermal separation and recycling. Invoking thermal separation necessitated studying the vapour-liquid equilibrium (VLE) of the chemical components in question. Additionally, some possible process flowsheets were simulated by simplifying the fractionation section while the thermal separation and recycling parts were rigorously modelled.

Based on the energy consumption data from the simulated process flowsheets, the imidazolium-based IL appears to be more economical while the DIL consumes less energy as compared to the SIL.

Keywords Ionic liquid, biomass fractionation, SIL, DIL, VLE, CPE, flashing, chemical equilibrium, phase equilibrium, process simulation, multicomponent distillation.

ACKNOWLEDGEMENTS

Verily, all expressions of appreciation ultimately belong to the Creator, Sustainer and Cherisher of humankind and the universe, and thus, I say AlhamduliLLAH.

This thesis is written within the Chemical Engineering Research Group, as such, the hospitality of every member of the group is sincerely appreciated; the foods at the get-togethers, the smiling faces along the corridor, the comments and suggestions during the KELA meetings, the expertise advices and also the friendly administrative services.

Furthermore, I am grateful to Professor Ville Alopaeus for giving me the opportunity to work in his research group and the Fubio JR2 project. His comments during the project and KELA meetings are all appreciated. Dr. Kaj Jakobsson also deserves big thanks for overseeing the work, giving valuable and motivating advices and above all, for making the working environment very enjoyable. I am also grateful to M. Sc. Penttilä Anne for proof-reading the first version of the literature review.

Lastly, Finnish Bioeconomy Cluster (FIBIC) is duly thanked for funding the project.

LIST OF NOMENCLATURE

Symbols

C_p^{IG}	Specific heat capacity of ideal gas (J/mol-K)
C_p^L	Specific heat capacity of liquid (J/mol-K)
f_i^V	Fugacity of ith component in vapour mixture (Pa)
f_i^L	Fugacity coefficient of ith component in vapour mixture (Pa)
F	Feed flow (mol/s)
G^E	Gibbs excess energy (Joule)
ΔG^o	Standard state Gibbs free energy change (Joule)
$\Delta_r G^o$	Standard state Gibbs free energy change of reaction (Joule)
$\Delta_f G_i$	Gibbs free energy of formation of ith component (J/mol)
$\Delta_r G$	Gibbs free energy change of reaction (Joule)
$\Delta_f G_i^o$	Standard Gibbs free energy of formation of ith component (J/mol)
G_{ij}	NRTL interaction parameter
Δg_{ij}	Interaction energy parameter (J/mol)
$\Delta_f H_i^o$	Standard enthalpy of formation of ith component (J/mol)
H	Unit holdup
ΔH_{vap}	Enthalpy of vaporization (J/mol)
K_{eq}	Chemical equilibrium constant
L	Liquid flow (mol/s)
n_i^o	Component ith initial amount (mol)
n_i	Component ith amount (mol)
p_i^{SAT}	Saturated vapour pressure of ith component (Pa)
p^V	Vapour phase pressure (Pa)
p^L	Liquid phase pressure (Pa)
R	Gas constant (J/mol-K)
$\Delta_f S_i^o$	Standard entropy of formation of ith component (J/mol)

T	Temperature (K)
T^V	Vapour phase temperature (K)
T^L	Liquid phase temperature (K)
v	Molar volume (m^3/mole)
V	Vapour flow (mol/s)
x_i	Mole fraction of ith component in liquid phase
y_i	Mole fraction of ith component in vapour phase
z_i	Mole fraction of ith component in the feed
Z	Compressibility factor

Subscripts

i	ith component
j	jth component

Superscripts

E	Excess thermodynamic property
L	Liquid
SAT	Saturated thermodynamics property
V	Vapour

Greek letters

μ_i^V	Chemical potential of ith component in vapour phase
μ_i^L	Chemical potential of ith component in liquid phase
μ_i^o	Standard chemical potential of ith component
τ_{ij}	NRTL interaction parameter
α_{ij}	NRTL non-randomness parameter
ε	Extent of reaction

ν_i	ith component stoichiometric coefficient
ϕ_i^V	Fugacity coefficient of ith component in vapour mixture
ϕ_i^L	Fugacity coefficient of ith component in liquid mixture
ϕ_i^{SAT}	Fugacity coefficient of saturated vapour pressure
γ_i	Activity coefficient of ith component

Abbreviations

ASOG	Analytical solution of groups
CPE	Chemical and phase equilibrium
DBU	1,8-Diazabicyclo[5.4.0]undec-7-ene
DIL	Distillable ionic liquid
[emim][OAc]	1-ethyl-3-methylimidazolium acetate
EOS	Equation of state
IL	Ionic liquid
NRTL	Non-random two-liquid model
RTIL	Room temperature ionic liquid
SIL	Switchable ionic liquid
TMG	1,1,3,3-tetramethylguaidine
UNIFAC	Uniquac functional activity coefficients
UNIQUAC	Universal quasichemical
VLE	Vapour-liquid equilibrium

TABLE OF CONTENTS

1 Introduction

Biomass and bioenergy have been increasingly researched due to reasons, such as increased environmental awareness and the need to expand the capacity of bio-based industries. Biomass contains stored energy that can be harnessed via the concept of biorefinery to produce energy and useful industrial chemicals. In order to harness this stored energy for bioenergy and biochemical production, biomass has to be separated in to its basic constituents—cellulose, hemicelluloses and lignin.

Separation of biomass components, biomass fractionation, is a practice which has been accomplished with various techniques in different fields of application. Methods, such as steam explosion; hot water extraction; and kraft pulping are known to employ harsh conditions, toxic chemicals and even incur some biomass component loss, mainly hemicellulose (Tan and Lee, 2012). With the upsurge of environmental awareness and sustainable practices, greener and sustainable technology is always being sought. Ionic liquids (ILs) seem to be promising with regard to the required characteristics demanded of a green solvent. Consequently, several published papers have been dedicated to investigating and reporting the dissolution of lignocellulosic material with ILs on a laboratory scale (Anugwom et al., 2012; Hyvarinen et al., 2011; Kilpeläinen et al., 2007; King et al., 2011; Mäki-Arvela et al., 2010; Wei et al., 2012). In order to recover used ILs from the dissolved components, there are a number of options whose applicability depends on the properties of the IL in question.

Thermally-driven separation and recycling is an option applicable to all the type of ILs. This has been reported mainly in papers based on laboratory experience and theoretical opinion (King et al., 2011; Mäki-Arvela et al., 2010; Ober and Gupta, 2012). From an industrial point of view, ILs recyclability is vital to making potential ILs applications economical. Additionally, for ionic liquids to be fully regarded as green and sustainable solvents, their effective recyclability must be clearly defined. In light of these facts, the need to identify the most economical and efficient IL becomes clear.

The task of identifying the most promising IL with respect to thermally-driven separability and recyclability requires a thorough thermodynamics study—mainly vapour-liquid equilibrium (VLE). Admittedly, a number of VLE and simulation studies involving ILs have been published; however, most of them do not examine the ILs of interest in biomass fractionation (Bedia et al., 2013; Döker and Gmehling, 2005; Ferro et al., 2012; Hector et al., 2013; Römich et al., 2012). Moreover, no published worked has embarked on investigating the most promising of the ILs used for biomass fractionation.

Thus, the goal of this thesis is to identify the most promising type of IL via modelling and simulation of the biomass fractionation process. The biomass fractionation process shall be modelled with different ILs with the main focus being on the separation and recycling section. This thesis will start with a brief presentation on ILs and their characteristics as potential green solvent. Following ILs description, the next chapter will present an overview of the reported biomass dissolution cases with the aim of identifying ILs of choice in biomass fractionation and their dissolved components. Furthermore, chapter 3 will be dedicated to the thermodynamics framework needed for VLE modeling.

Additionally, chapter 3 shall consider isothermal flash model. Finally, the last chapters will cover the modelling practicalities, including fitting parameters of models, the development of recycling schemes and the simulation of the developed schemes in Aspen Plus as well as the comparison of results.

I LITERATURE PART

2 Ionic Liquids and Biomass Fractionation

The seemingly potential green and designer solvent popularly known as ionic liquids (ILs) will be discussed in this chapter. The basic idea behind its functionality and characteristics will be briefly mentioned in Section 2.1 while Section 2.2 will be focused on the fractionation of lignocellulose material with the goal of identifying the content of the extract stream in biomass fractionation process. The last section shall examine the recycling solutions currently applied in applications employing ionic liquids.

2.1 Ionic liquids

The term ionic liquids generally refer to ionically bonded compounds existing as liquid below 100 degree Celsius (Li et al., 2010). ILs that exist as liquid below 25 degree Celsius are specifically denoted as room temperature ionic liquids (RTILs). Ionically bonded compounds are known for their high melting point as they are symmetrically held by electrostatic force; as such, they exist as solid for a wide range of temperature. ILs, however, owe their liquid state to the effect of the bond-weakening conditions caused by ions size and structural irregularity. Consequently, ILs are formed when a large and asymmetrically structured organic cation is bonded to either an organic or inorganic anion (Mäki-Arvela et al., 2010). The choice of cation-anion combination in synthesizing ILs is numerous, thus hundreds of ILs have been synthesized in

the laboratory. Some of the commonly used cation-anion options alongside some frequently employed ILs in biomass fractionation are shown in Figure 1 and Figure 2 respectively. The choice of cation-anion combination is usually exploited to tailor properties of synthesized ILs as desired; hence, ILs are also referred to as designer solvent (Safarov et al., 2012).

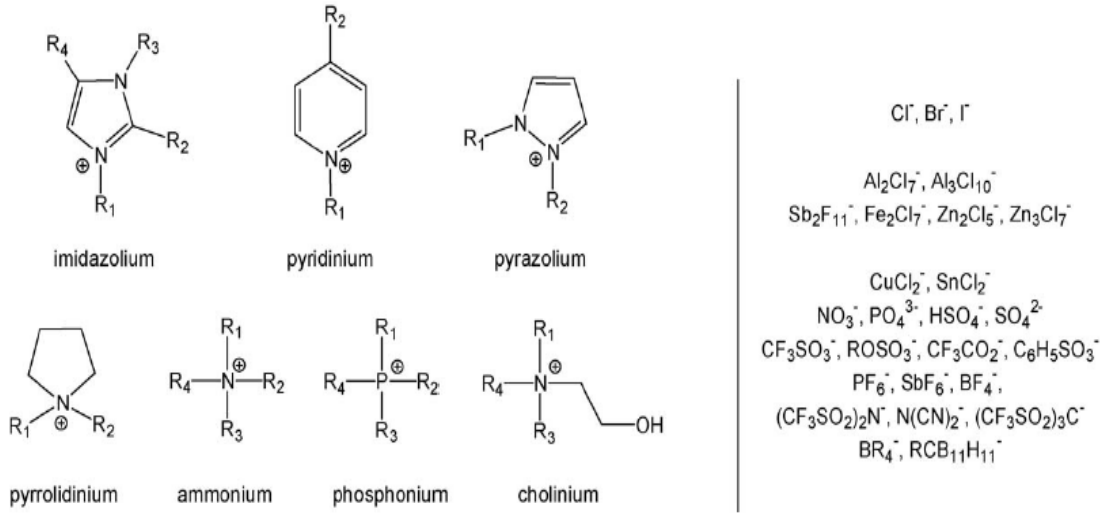

Figure 1: Commonly used cations and anions in ILs.

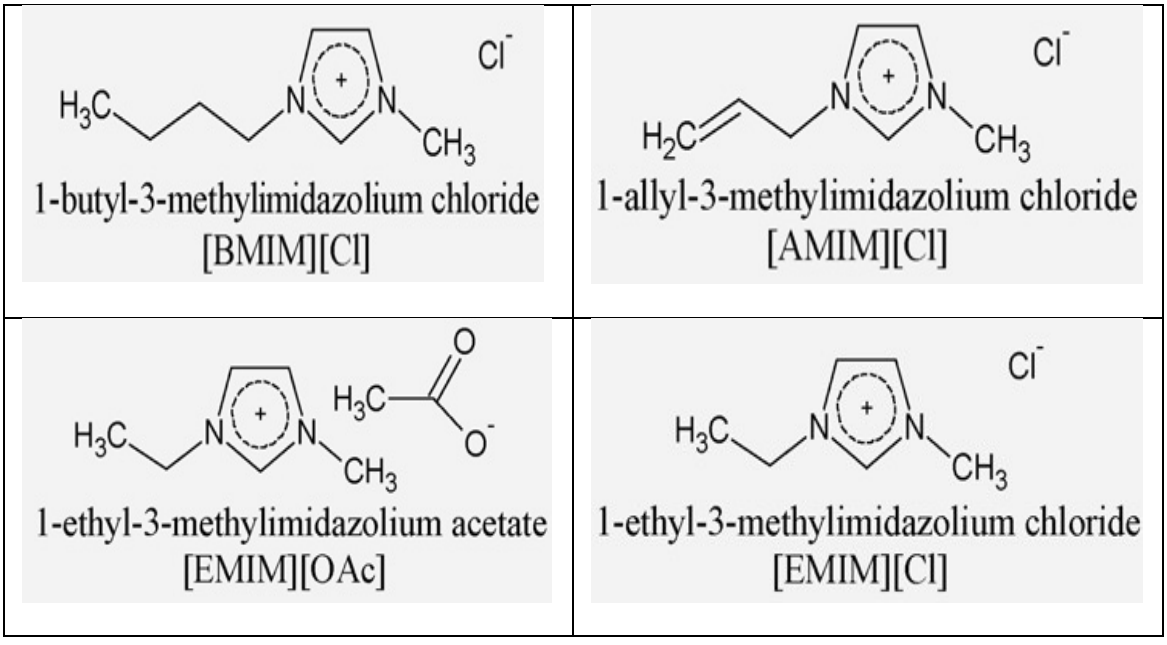

Figure 2: Common ionic liquids for biomass fractionation.

Generally, ionic liquids are characterized by high conductivity, low vapour pressure, low flammability and high thermal stability. These characteristics of ILs are not farfetched considering the strong nature of the liquid pool interaction. For instance, the observed high conductivity can be attributed to the presence of mobile charges in the pool while the low flammability and vapour pressure of ILs can be attributed to the high energy required for an ion or ion-pair to escape from ionic liquid pool. This low tendency of IL evaporation is particularly advantageous from the environmental point of view as air pollution from IL-using processes will be minimal or less likely to occur. (Mäki-Arvela et al., 2010).

2.2 Biomass fractionation with ionic liquid

Lignocellulose materials have been identified as a CO_2-neutral, renewable and sustainable source of bioenergy—mainly through biofuel production—and biochemicals. Due to these attractive qualities of lignocellulose materials, a lot of attentions have been focused on fractionating its components for applications. For instance, cellulose and hemicelluloses are being considered for biofuel production through enzymes digestion. (Tan and Lee, 2012)

With regards to separating biomass to its components with ionic liquids (ILs), several papers have been published identifying a number ILs with their various dissolution abilities (Anugwom et al., 2012; Hyvarinen et al., 2011; Kilpeläinen et al., 2007; King et al., 2011; Mäki-Arvela et al., 2010). Generally, ILs ranges in terms of their dissolution ability; some specifically dissolve a particular component while some can even dissolve the whole biomass altogether. Biomass dissolution ability of ILs is directly related to the basicity of its

hydrogen bonding (Mäki-Arvela et al., 2010). Additionally, ILs biomass dissolution strength reduces with increase in the size of the cation alongside its alkyl branching due to hindrance to hydrogen bonding formation. In combination with an appropriate cation, smaller anions enhance ILs dissolution strength. (Mäki-Arvela et al., 2010; Tan and Lee, 2012)

Summarily, a good IL candidate for cellulose dissolution would have a small polarizing cation together with an anion enabling attack of cellulose hydrogen bonding. For imidazolium based ILs, halides, formate and acetate are regarded as good anion candidate for cellulose solvent. As for lignin, the following ILs are identified as the most effective; 1-butyl-3-methylimidazolium trifluoromethanesulfonate and 1,3-dimethylimidazolium methylsulphate. In the case of biomass dissolution altogether, a general rule of thumb is that a good cellulose and lignin solvent can adequately dissolve wood as well (Mäki-Arvela et al., 2010). Nonetheless, 1-ethyl-3-methylimidazolium acetate is recognized to be the most suitable and promising IL amongst its imidazolium-based counterparts because of its relatively low dissolution temperature and toxicity as compared to its peer solvents. (Mäki-Arvela et al., 2010; van Spronsen et al., 2011)

Table 1 presents a list of various ILs and their dissolution ability as reported in published papers. Mäki-Arvela et al. (2010) in their review collected an exhaustive list of different ILs reported in the literature with their corresponding dissolution ability. Virtually, all the reported ILs were either for cellulose, lignin or wood dissolution.

It is also noteworthy that the dissolution of biomass and/or its components by ILs are non-derivatizing in nature, that is, no formation of new compounds (Mäki-Arvela et al., 2010). The interaction of ILs with biomass is solely intermolecular in nature, hence, merely depolymerizing the biopolymers. Furthermore, from applications point of view, ILs action on biomass weakens the crystal nature of cellulose making it easily hydrolyzed for further processing. In general, imidazolium-based ILs are the most commonly utilized ILs, however, that is not to say they are the only types of ILs synthesizable. In fact, in view of easy recycling, two new generations of ILs synthesized with organics base, such as, 1,8-diazabicyclo[5.4.0]undec-7-enium (switchable ILs) and 1,1,3,3-tetramethylguaidine (distillable ILs) are fast becoming more promising options (Anugwom et al., 2012; King et al., 2011).

TABLE 1: Popular ILs for cellulose and wood dissolution.

IONIC LIQUIDS	
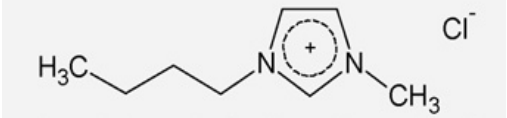 1-butyl-3-methylimidazolium chloride [BMIM][Cl]	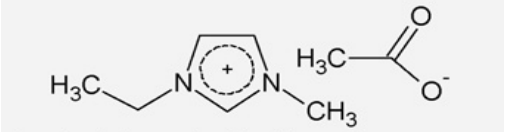 1-ethyl-3-methylimidazolium acetate [EMIM][OAc]
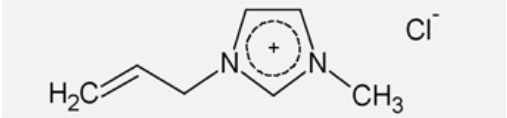 1-allyl-3-methylimidazolium chloride [AMIM][Cl]	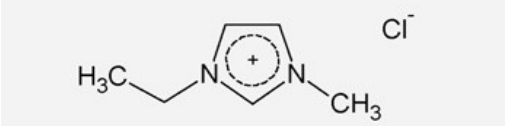 1-ethyl-3-methylimidazolium chloride [EMIM][Cl]

2.3 Ionic liquid recycling

Following biomass fractionation with an IL, the resulting extract is a multicomponent liquid mixture. These components are dissolved biomass components—cellulose, hemicellulose and lignin—, the employed IL and probably some degraded biopolymers, depending on the fractionating condition, alongside possible of impurities. Obviously, this mixture will vary in composition and components as different ILs differ in their dissolution ability of biomass components. Priority is given to recovering biomass dissolved component(s) as recovering them is the goal of the whole process. The most common recovery method reported in literature is to precipitate biomass dissolved components with an antisolvent such as water and/or methanol (ethanol in some cases). The precipitation is performed in turns and in different conditions for different components. (Mäki-Arvela et al., 2010; Tan and Lee, 2012; Wei et al., 2012)

Cellulose is commonly the first to be precipitated and filtered. Afterwards, lignin is precipitated in an acidic condition which can be attained by introducing CO_2 flow into the solution (Ober and Gupta, 2012). This approach of initiating acidic environment for lignin precipitation reduces the risk of introducing impurity into the system by the conventional usage of mineral acid. The last step is to evaporate the remaining antisolvent and water to recover the IL. A pictorial depiction of the typical procedure followed for IL recovery in the laboratory is shown in Figure 3.

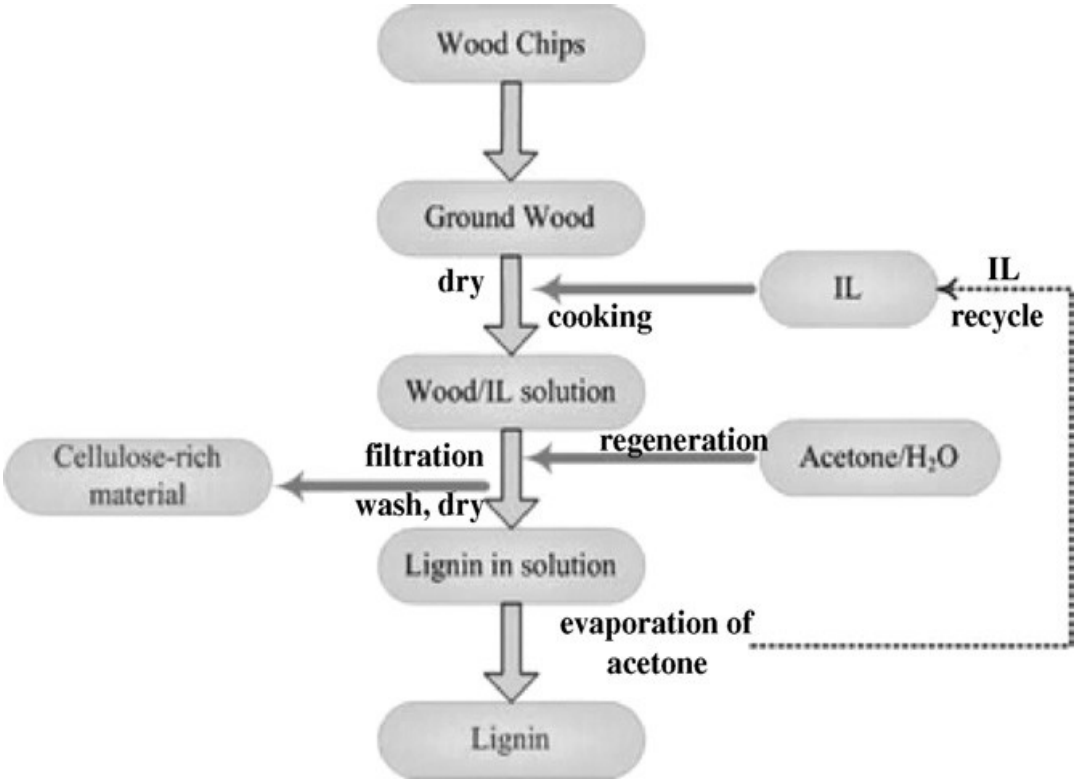

Figure 3: Overall chart of IL recycling in laboratory. (taken from Mäki-Arvela e.al . 2010)

Apart from precipitating the dissolved components with nonsolvents and subsequent filtration, immiscible inorganic solvents can also be used to separate and recover IL from the complex mixture. Vacuum distillation of IL is also applicable and in fact this option is very attractive because of the guaranteed purity of recovered ILs.

2.3.1 Ionic liquid distillation

Amongst the recycling options available for ionic liquids, distillation is an option applicable to ILs of all types. Additionally, this IL recovery approach guarantees better purity as the ILs distills to leave impurities behind. With regards to distillability of aprotic ILs, Earle et al. (2006) clears the air by reporting vapour pressure data for a number of imidazolium-based ILs. Protic

ILs are known to exist in equilibrium within their two different forms; the ion-pair charged form and dissociated neutral form (formed when the anion accepts proton from the cation). Consequently, the vapour formed upon vapourizing IL contains the neutral molecules which can be recombined. (Earle et al., 2006)

As for the aprotic family of ILs, the nature of their vapourization is controversial. Earle et al. (2006) concluded that the correct liquid-vapour transfer mechanism is by ion or ion aggregate volatilization without being specific about the vapour phase nature. José M. S. S. Esperança et al. 2010, however, favours phase transition by single ions transfer. They went on further to explain that neutral ion-pairs can dissociate at high temperatures in the vapour phase. Leal et al. (2007) also investigated the nature of ILs vapour phase. The results from their experiments established that neutral molecules and neutral ion-pairs are present in protic and aprotic vapour phases respectively. Figures 4 and 5 schematically summarize the arguments. (Earle et al., 2006; José M. S. S. Esperança et al., 2010; Leal et al., 2007)

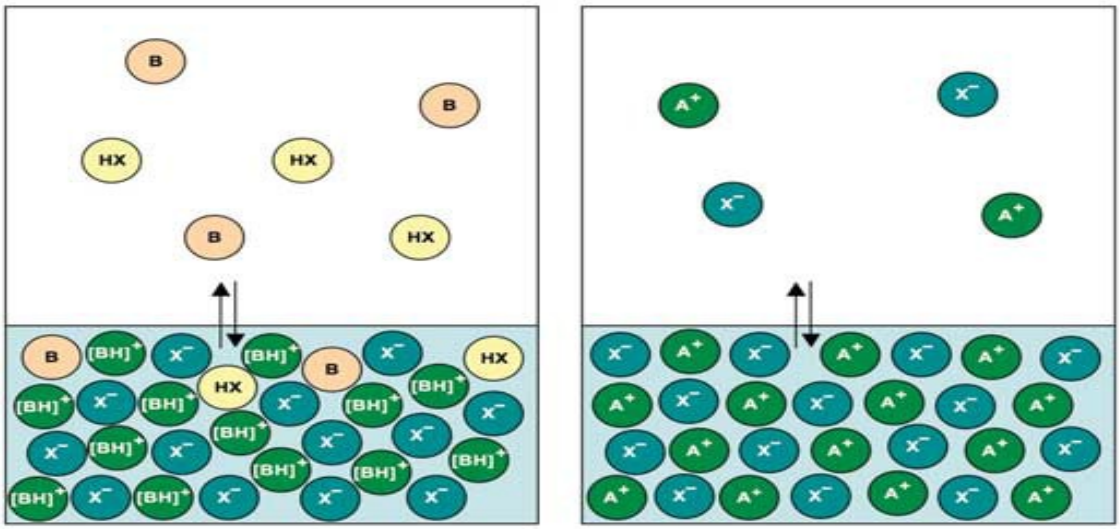

Figure 4: Schematic presentation of protic (left) and aprotic (right) IL vapourization.

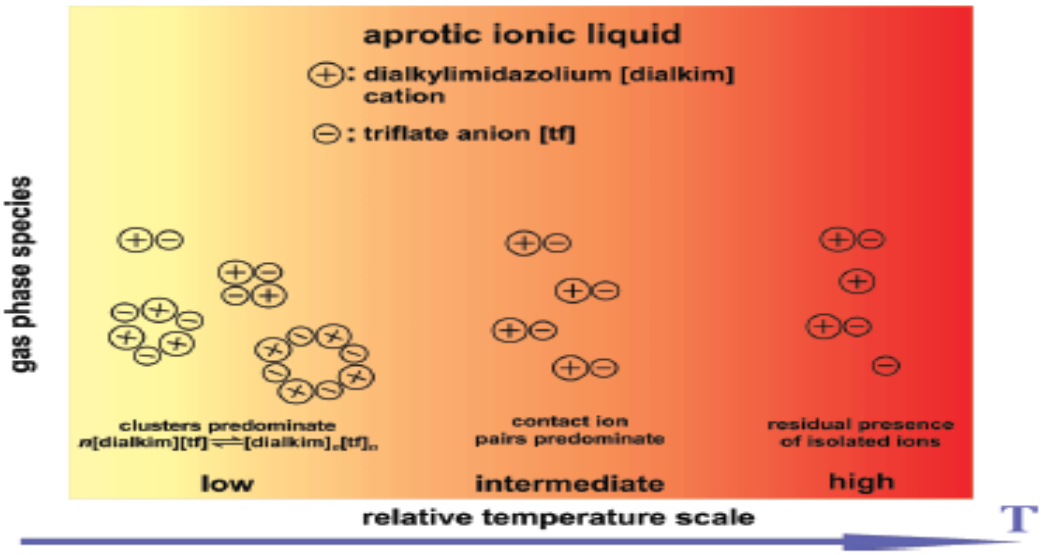

Figure 5: Possibilities of aprotic ILs vapour nature.

Following the explanations above, the traditional imidazolium based ILs can be distilled at high vacuum. Alternatively, BASF (2013) claimed the possibility of switching off—converting IL to neutral and easily distillable molecule—the traditional imidazolium based ILs. This procedure is easiest in a protonated IL as the cation is simply deprotonated to form an imidazole while the anion accepts the proton to form an acid as shown in Figure 6. (BASF, 2013).

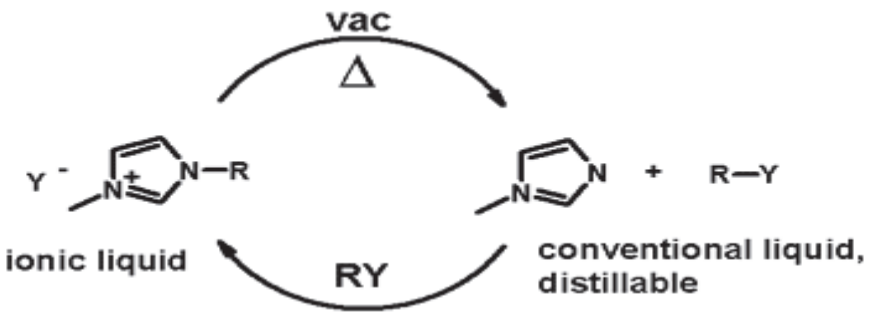

Figure 6. Protonated imidazolium IL switching off.

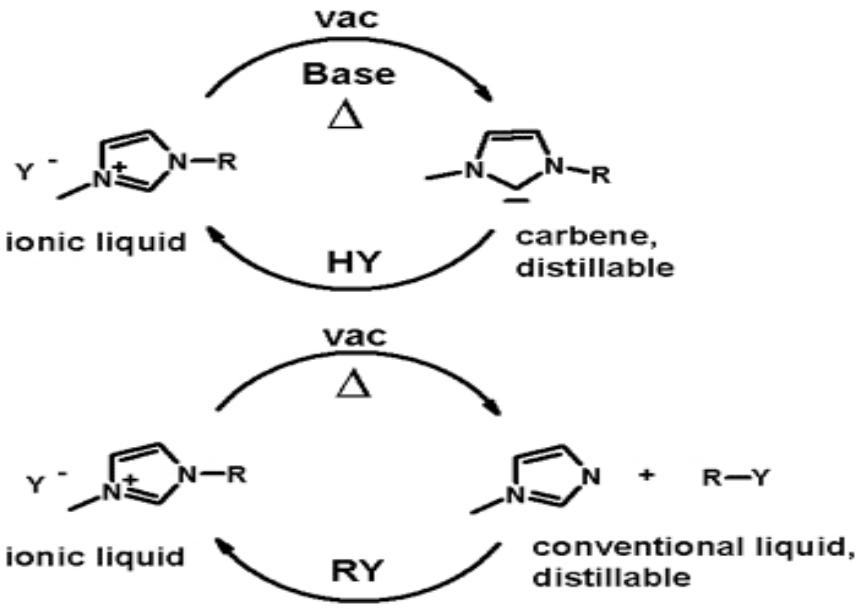

Figure 7: Formation of distillable carbenes and imidazole from alkylated ILs.

Figure 7 illustrates the switching off of alkylated imidazolium based ILs. This can be achieved either by thermal cleavage or in the presence of a base to form distillable imidazole and carbenes respectively. Imidazole and carbene can be distilled and reacted with an acid and an alkylating agent respectively to regenerate the IL in question.

The concept of ILs switching off and on has lead to a new generation of ILs specially referred to as switchable ionic liquids (SILs). SILs are synthesized from two molecular compounds and a gas stream (Anugwom et al., 2012). The ionic liquid behaviour of the mixture is switched on in the presence of the employed gas flow. Switching off these ILs simply requires stripping the solution of the gas stream. With respect to distillation, SILs can be easily switched off by distillation after biomass dissolution. The distilled molecular liquids are then recombined and switched on for the next round of biomass fractionation.

Anugwom et al. (2012) synthesized two SILs using alcohols (hexanol and butanol) and amidine (1,8-diazabicyclo[5.4.0]undec-7-enium)(DBU) in the presence of carbon dioxide. DBU-based SILs are capable of selectively dissolving hemicellulose. This is particularly interesting as hemicellulose is less discussed in terms of biomass component dissolution.

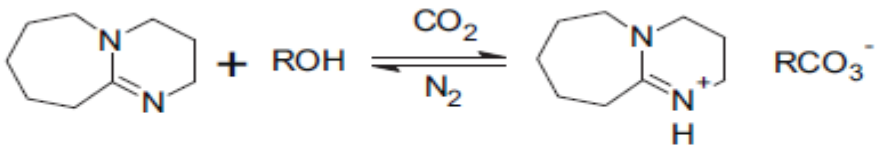

Figure 8: Illustration of SIL formation from an alcohol and DBU.

Similarly, another easily distillable new generation of ILs is the based on 1,1,3,3,-tetramethylguaidine (TMG)—an organic base—and organic acids such as formic and acetic acid (King et al., 2011). The mixture act is capable of dissolving cellulose and can dissociate to the starting acid and base (TMG) at about 140 degree Celsius temperature. With the aid of temperature, a TMG-based IL can have its equilibrium shifted to the right to favor production of the starting molecular acid and base. These starting components can be easily distilled and recombined for recycling. King et al. (2011) reported 99% purity of recovered TMG-based IL pointing out its superiority to 95% purity of imidazolium-based ILs reported by BASF (2013).

3 Theoretical Background of Vapour-Liquid Equilibrium

Ionic liquid purification by temperature swing processes requires an understanding of vapour-liquid equilibrium (VLE) behaviour of the IL solution in question. This understanding necessitates mathematically describing (modelling) VLE of the system in consideration for general simulation purpose. Additionally, an isothermal flashing model and an expedient solution algorithm are required for phase composition and fraction determination within the simulation. To start with, the traditional VLE modeling approach will be reviewed. The next subheading shall consider ionic liquids VLE modelling available in literature. Lastly, flashing model and the solution algorithm will be treated. This presentation will be limited in terms of equations as the relevant thermodynamics equations are compiled in the appendices. Detailed description of the terminologies used in this chapter can be found in chemical engineering thermodynamics books for thorough understanding.

3.1 General vapour-liquid equilibrium modelling

Vapour-liquid equilibrium modelling is an important concept in chemical engineering because of its importance in distillation and gas absorption—the most matured and used unit operations. Prior to equilibrium description of vapour/gas-liquid systems, it is essential to present the basic variables required to describe each of the phases; vapour/gas and liquid phase.

Vapour phase: In a multicomponent vapour system with the following state variables, p, v, and T, denoting pressure, molar volume and temperature respectively, the following equations are valid;

$$p_i = y_i p \tag{3-1}$$

In equation (3-1), y_i and p_i represent the ith component mole fraction and partial pressure respectively.

$$p = \sum p_i \tag{3-2}$$

In order to account for non-ideal behavior in real systems, a modified partial pressure is defined for real gases as fugacity, f_i^V. Fugacity is a multiple of component partial pressure and fugacity coefficient— Φ_i^V —defined as follows

$$f_i^V = \Phi_i^V p_i = \Phi_i^V y_i p \tag{3-3}$$

Fugacity coefficient can be estimated from equation (3-4), either in pressure or volume explicit form.

$$\ln(\Phi_i^V) = \frac{1}{RT}\int_{v=\infty}^{v=\frac{zRT}{p}} \left[\frac{RT}{v} - n\left(\frac{\partial p}{\partial n_i}\right)_{T,v,n_{j\neq i}}\right] dv - \ln(z) \tag{3-4}$$

In equation (3-4), volume explicit fugacity coefficient expression, the pressure as a function of other state variables can be taken from any of the equation of state (EOS) models. Some EOS models alongside constant parameters mixing rules for mixtures are presented in the appendix A.

Liquid phase: The total vapour pressure above a liquid mixture can be related to its pure components saturated vapour pressure, p_i^{sat}, using Raoult's law as defined below;

$$p = \sum x_i p_i^{sat} \tag{3-5}$$

Just as in the vapour phase, accounting for non-ideality demands introducing a coefficient. Either fugacity coefficient or activity coefficient, γ_i, can be introduced. For each of the cases, the corresponding component liquid phase fugacity can be defined as follows;

$$f_i^L = \Phi_i^L p_i = \Phi_i^L x_i p \quad \text{(Fugacity coefficient method)} \tag{3-6}$$

$$f_i^L = x_i \gamma_i \Phi_i^{sat} p_i^{sat} \exp\left(\int_{p_i^{sat}}^{p_{ref}} {}^{V}/_{RT}\, dp\right) \quad \text{(Activity coefficent method)} \tag{3-7}$$

In equation (3-7), Φ_i^{sat} represents the fugacity coefficient of the pure component saturated vapour pressure and the exponential term is a pressure correction term popularly known as the Poynting correction factor. Pure component vapour pressure can be calculated from models such as Antoine, Wagner, and Cox models amongst others, having fitted the model parameters with experimental data. Some vapour pressure models are presented in the appendix B.

The use of activity coefficient model captures nonideality introduced by molecular interaction in the liquid phase. In essence, activity coefficient model definition requires components fugacity to approach pure components

saturated vapour pressure at the operating temperature and pressure condition as components mole fraction and activity coefficient approach unit. The formulation is known as symmetrical definition. Symmetrical definition is not feasible for cases where gas, solid, or ionic species represents pure component at the defined standard state condition. The stated infeasibility is due to the fact that these species possess no vapour pressure. In such cases, a nonsymmetrical formalism is employed. Nonsymmetrical formulation uses standard state as the dissolved component at infinite dilution in an appropriate solvent. Thus, the standard state fugacity is the Henry's law constant as the component mole fraction and activity coefficient approach zero and unity respectively.

In order to calculate activity coefficient, a number of models such as Wilson, NRTL, and UNIQUAC are commonly used to represent the Gibbs excess energy in equation (8).

$$\ln\gamma_i = {}^{1}/_{RT}\left(\frac{\partial G^E}{\partial n_i}\right)_{T,p,n_{i\neq j}} \tag{3-8}$$

These models express excess Gibbs energy as a function of components mole fractions, system temperature and interaction parameters of components. The interaction parameters can be determined by fitting the model equation to relevant experimental data. Furthermore, there are also some special activity coefficient models with some additional terms meant to account for ionic interactions in electrolyte systems. Moreover, in the absence of experimental data, UNIFAC or ASOG which are based on group contribution method can be applied. Appendix C is dedicated to presentation of commonly used activity coefficient models.

Vapour-Liquid equilibrium: Equilibrium condition in a closed multicomponent and multiphase system can be defined by the condition of minimum Gibbs energy and maximum entropy. These postulates can be used to establish equality of temperature, pressure and chemical potential in all of the phases present in the system. These equality conditions are referred to as thermal, mechanical and chemical or material equilibrium conditions sequentially. For a liquid-vapour system, they can be mathematically expressed as follows;

$$T^V = T^L \tag{3-9}$$

$$p^V = p^L \tag{3-10}$$

$$\mu_i^V = \mu_i^L \tag{3-11}$$

In chemical engineering applications, equality of chemical potentials expressed in equation (3-11) is usually replaced by fugacity equality.

$$f_i^V = f_i^L \tag{3-11b}$$

In employing fugacity equality relationship to predict the phase equilibrium, two approaches are common; phi-phi method and phi-gamma method. In the phi-phi approach, both liquid and vapour phase fugacities are expressed using the fugacity coefficient method. Phi-gamma on the other hand applies activity coefficient for the liquid phase and fugacity coefficient for the vapour phase. Activity coefficient method is known to model liquid phase more accurately,

hence, it is more in use. The general fugacity equality expression at equilibrium for gamma-phi method is presented in equation (3-12).

$$\Phi_i^V y_i p = x_i \gamma_i \Phi_i^{sat} p_i^{sat} \exp\left(\int_{p_i^{sat}}^{p_{ref}} \frac{v}{RT} dp\right) \quad (3\text{-}12)$$

In a non-reactive system, the expression of fugacity equality in all phases is sufficient for VLE modeling. In a reactive liquid mixture, however, it is required to invoke Gibbs energy minimization for all reactions alongside the fugacity equality equation. In other words, chemical and phase equilibrium are coupled together and both conditions must be fulfilled. Equation (3-13) presents the expression for Gibbs free energy at equilibrium which basically models chemical equilibrium in the reactions.

$$dG = \sum_i \mu_i dn_i \quad (3\text{-}13)$$

Modeling systems with coupled chemical and phase equilibrium (CPE) requires finding solution to equations (3-12) and (3-13). Solving these equations can be done in two ways; formulation and minimization of Gibbs energy or solving the nonlinear simultaneous equations (Avami and Saboohi, 2011; Bonilla-Petriciolet et al., 2008). Under the umbrella these solution approaches, different researchers have also used different techniques and algorithms to achieve their goals in an expedient manner. (Seider and Widagdo, 1996; Ung and Doherty, 1995; Ung and Doherty, 1995)

Considering the following reaction in a liquid mixture;

$$v_a A_L + v_b B_L + \cdots \rightarrow v_c C_L + v_d D_L \cdots \quad (3\text{-}14)$$

$$n_i = n_i^0 + \nu_i \varepsilon \tag{3-15}$$

Equation (3-15) describes the change in mole for each of the reacting components. Furthermore, utilizing the equation for Gibbs free energy at equilibrium—equations (3-13)—,it is easy to establish the traditional equilibrium constant expression—equation (3-16).

$$\Delta G^0 = \sum_i^N \nu_i \mu_i^0 = -RT \times \ln \prod (\gamma_i x_i)^{\nu_i} \tag{3-16}$$

Solving equations (3-12) and (3-16) with composition summation constraints is the so called simultaneous equation solving method for CPE. Gibbs minimization procedure, on the other hand, minimizes Gibbs function for the system with atom balance of the components as constraints.

3.2 Ionic liquids' vapour-liquids equilibrium modelling

Vapour-liquid equilibrium (VLE) modeling in ILs systems will naturally require novel adjustment to the traditional methods applied to molecular liquids as a result of its complex nature. Compounding this complexity is the fact that the solution and vapour chemistry of ILs is still debatable (Wang et. al 2011).

In general, published works related to VLE measurement and modeling of ILs-containing systems have made varying assumptions about the potential green solvent's chemistry. These assumptions can be categorized into three: 1. normal molecular liquids; 2. completely dissociated in liquid phase; 3. partly dissociated. Models making the first assumption surprisingly dominate the literature with acceptable VLE data prediction. Such models commonly utilize

different equation of state (EOS) models for the vapour phase and activity coefficient for liquid phase. Peng-Robinson is by far the most used EOS while NRTL and UNIQUAC are the popular options in the liquid phase. (Alvarez and Saldaña, 2012; Anderko et al., 2002; Kato et al., 2004; Maia et al., 2012; Wang and Anderko, 2011)

The second category of assumption simply applies the electrolyte-NRTL for modeling the dissociated cations and anions while the remaining part follows the conventional practice. The category, also known as the speciation model, is a rather rigorous model that includes additional terms in the excess Gibbs expression for estimating activity coefficient. The additional terms, as shown in equation (3-17) are meant to account for the electrostatic (LR), ion-ion (II) and ion-pair interactions (II) within the liquid phase.

$$\frac{G^E}{RT} = \frac{G^E_{LR}}{RT} + \frac{G^E_{II}}{RT} + \frac{G^E_{SR}}{RT} \tag{3-17}$$

The short range term can be modeled with any activity coefficient methods—NRTL, UNIQUAC amongst others. The detailed expressions of the extra terms are gathered in equations (3-17a) to (3-17i). In addition to the elongated Gibbs terms, chemical equilibrium is simultaneously solved in this model.

$$\frac{G^E_{LR}}{RT} = -\left(\sum_I n_i\right)\frac{4A_x I_x}{\rho}\ln\left(\frac{1+\rho I_x^{1/2}}{\sum_i x_i[1+\rho(I^0_{x,i})^{1/2}]}\right) \tag{3-17a}$$

$$I_x = (1/2)\sum_i x_i z_i^2 \tag{3-17b}$$

$$A_x = \frac{1}{3}(2\pi N_A d_s)^{1/2}\left(\frac{e^2}{4\pi\varepsilon_0\varepsilon_s k_B T}\right)^{3/2} \quad (3\text{-}17c)$$

$$\frac{G_{II}^{EX}}{RT} = -\left(\sum_I n_i\right)\sum_i\sum_j x_i x_j B_{ij}(I_x) \quad (3\text{-}17d)$$

$$B_{ij}(I_x) = B_{ji}(I_x) \quad (3\text{-}17e)$$

$$B_{ii} = B_{jj} = 0 \quad (3\text{-}17f)$$

$$B_{ij}(I_x) = b_{ij} + c_{ij}\exp\left(-\sqrt{I_x + a_1}\right) \quad (3\text{-}17g)$$

$$b_{ij} = b_{0,ij} + b_{1,ij}T + {}^{b_{2,ij}}/_{T} \quad (3\text{-}17h)$$

$$c_{ij} = c_{0,ij} + c_{1,ij}T + {}^{c_{2,ij}}/_{T} \quad (3\text{-}17i)$$

In general, it was agreed that VLE modeling of ILs does not necessarily have to be detailed as the rigorous speciation model to produce acceptable results (Wang and Anderko, 2011). Comparable results are obtainable by merely using the molecular liquids assumption (Maia et al., 2012; Wang and Anderko, 2011). Wang et al. (2011) noted that the speciation model is specifically important when transport properties are to be simulated.

3.3 Reactive flash model and solution algorithms

Flashing calculations are fundamentally important in chemical engineering as they are required for phase, composition, temperature and pressure determination within process simulation. Depending on the complexity of a process, its simulation can warrant calling flash calculations tens to thousands of times. Thus, the importance of an expedient solution algorithm becomes apparent as the speed of its solution directly tells on the overall process simulation time.

Solving reactive flash model is quite complicated because of the coupled nature phase and chemical equilibrium. Nonetheless, most of the published works have tried to maintain the traditional form of Rachford-Rice formulation (Pérez Cisneros et al., 1997; Ung and Doherty, 1995). A number of other algorithms are based on Gibbs minimization (Avami and Saboohi, 2011). Other groups of researcher have employed composition transformation to reaction invariant variables (Bonilla-Petriciolet et al., 2008; Jaime-Leal et al., 2012; Ung and Doherty, 1995). The latter method is particularly beneficial as the problem dimensionality is reduced making phase diagrams construction more feasible.

Presented below is the isobaric isotheral flash problem based on Ruiz et. al. (2006). Consider a reactive flash unit with a reaction and C number of components. Assuming F, L, V, H, xi, yi, zi, ε, and vi denote feed flow, liquid flow, vapour flow, unit holdup, liquid phase ith component composition, vapour phase ith component composition, feed ith component composition, reaction extent and ith component stoichiometry coefficient in reaction sequentially. The following formulation can be written for the system.

$$Fz_i = Lx_i + Vy_i - Hv_i\varepsilon \qquad (3\text{-}18)$$

$$y_i = K_i x_i \qquad (3\text{-}19)$$

$$\sum_i^C x_i = 1 \qquad (3\text{-}20a)$$

$$\sum_i^C y_i = 1 \qquad (3\text{-}20b)$$

$$R_i = Hv_i\varepsilon \qquad (3\text{-}21)$$

Rearranging equations (3-17) to (3-21) can easily yield equations (3-22) and (3-23)

$$x_i = \frac{z_i + \frac{R_i}{F}}{\frac{L}{F} + \frac{V}{F}K_i} \qquad (3\text{-}22)$$

$$y_i = K_i \frac{z_i + {R_i}/{F}}{{L}/{F} + {V}/{F}K_i} \qquad (3\text{-}23)$$

Furthermore, equation (3-20) – (3-19) results in equation (3-24).

$$\sum_i^C \frac{z_i + {R_i}/{F}}{{L}/{F} + {V}/{F}K_i}(K_i - 1) = 0 \qquad (3\text{-}24)$$

With the definition of stream ration as presented below, a modified form of Rachford-Rice equation—equation (3-26)—can be derived.

$$(\sum_i^C R_i)/F = \vartheta \qquad (3\text{-}25)$$

If ${V}/{F} = \theta$ and ${L}/{F} = 1 - \vartheta - \theta$

Then, $f(\theta) = \sum_i^C \frac{z_i + {R_i}/{F}}{(1-\theta-\vartheta)+\theta K_i}(K_i - 1) = 0 \qquad (3\text{-}26)$

The derivative of f(theta) is presented in equation (3-27)

$$f'(\theta) = -\sum_i^C \frac{z_i + {}^{R_i}/_F}{[(1-\theta-\vartheta)+\theta K_i]^2}(K_i - 1)^2 \qquad (3\text{-}27)$$

If the feed stream alongside the temperature and pressure at equilibrium are known; theta—the vapour to feed ratio— can be solved from equations (3-26) and (3-27) using Newton's method or iterative substitution method. Theta can be solved in the inner loop while the equilibrium compositions are estimated in the outer loop following the standard non-reactive algorithm.

II APPLIED PART

4 Vapour-Liquid Equilibrium Modelling of Ionic Liquids

The previous chapter discussed in detail, the theoretical concept of vapour-liquid equilibrium. In continuation, this chapter shall apply these VLE concepts to the ILs of interest for eventual thermal separation and recyclability analysis. The focus here is to present the assumptions and the practicalities employed in modelling of the VLE and necessary physical properties for the ILs of interest. Section 4.1 shall focus on ionic liquids originated from imidazolium cation, while Section 4.2 combines the case of distillable and switchable ionic liquids.

4.1 Modelling of imidazolium-based ionic liquid

According to the discussion on imidazolium-based ILs dissolution of biomass treated in section 2.2 of chapter 2, it was concluded that 1-ethyl-3-methylimidazolium acetate ([emim][OAc]) is the most promising solvent for lignocellulosic materials amongst its peers. This conclusion was based on the following attributes of [emim][OAc]: the ability to dissolve biomass at a relatively milder condition, tolerance to about 10 wt% of antisolvent (water in particular) without significant affect on its dissolution ability and the nontoxic nature due to its organic anion. (Mäki-Arvela et al., 2010)

In light of the acclaimed superiority of [emim][OAc], the VLE modelling performed is solely based on [emim][OAc] as the long term goal is to identify

the most promising IL for biomass fractionation via rigorous analysis of the thermal separation and recycling section of the overall process. Rigorous modelling of thermally-driven separation demands good understanding of the VLE of the chemical systems in consideration. Hence, the VLE modelling for IL-antisolvent system is the goal of this section.

For the purpose of the modelling task performed, [emim][OAc] is the IL while water is the antisolvent. It is desirable to investigate the VLE for the chemical system with other alcoholic antisolvent; however, this was hampered by the nonavailability of adequate data as will be discussed later in this chapter. Furthermore, for the VLE modelling purpose the gamma-phi model is utilized while IL is treated as molecular specie. This modelling approach is favoured as it had consistently yielded acceptable results in earlier publications about ILs (Döker and Gmehling, 2005; Kato et al., 2004; Revelli et al., 2010). Besides, increasing the model hierarchy by considering IL speciation will demand more thermodynamics data which are not available. Of course, such needed thermodynamics data can be optimized, but once again, there are no adequate data for the optimization to ensure thermodynamics consistency.

Furthermore on the modelling assumptions, an ideal vapour is assumed throughout this modelling. Likewise, the Poynting factor and fugacity coefficient of the saturated vapour pressures were neglected based on the assumption of moderate pressure condition. With the stated assumptions above, the gamma-phi equation can be reduced to equation 4-1. In order to proceed, the saturated vapour pressure and the liquid activity coefficient parameters are needed. Due to nonavailability of measurement data, negligible values or even naught are commonly assumed for ILs vapour pressure for the

purpose of VLE modelling (Döker and Gmehling, 2005; Revelli et al., 2010). In this work, some infinitesimal values were employed to fit the vapour pressure correlation for the IL. Equation 4-2 and Figure 9 represent the least square-fitted correlation and the graphical depiction of the correlation respectively.

$$y_i p = x_i \gamma_i p_i^{sat} \tag{4-1}$$

$$\ln p_{IL}^{sat} = 38.97 - \frac{15544.40}{T} \tag{4-2}$$

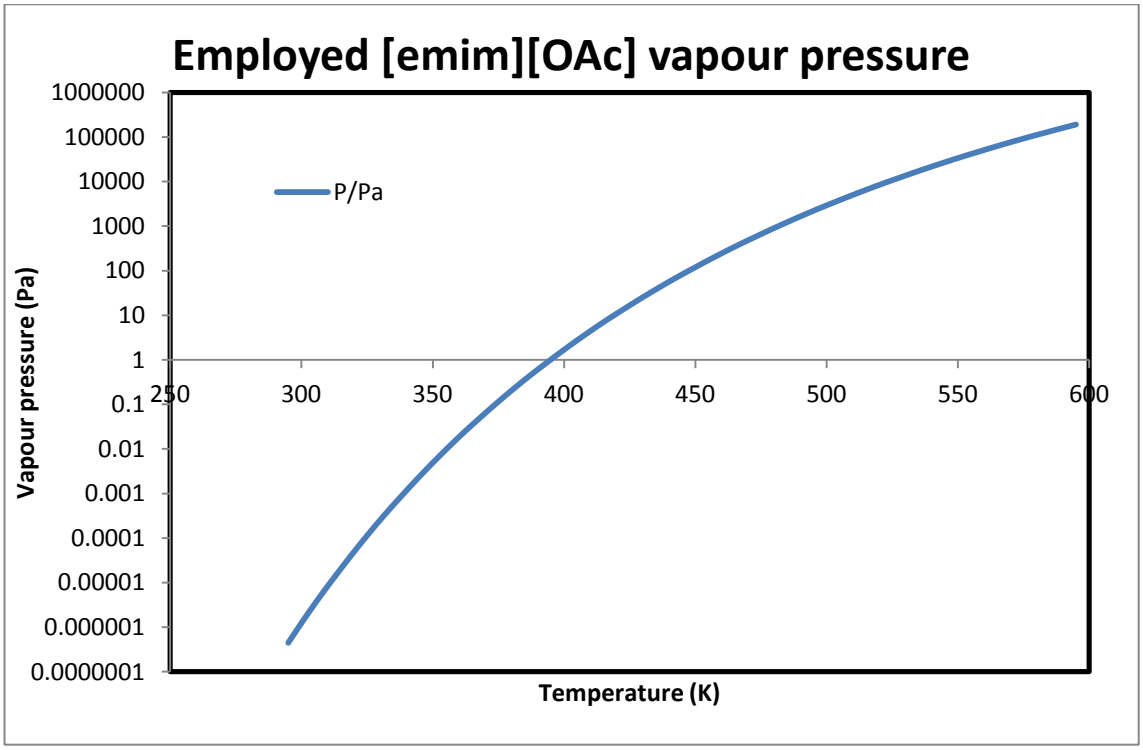

Figure 9: Semilog plot of vapour pressure of [emim][OAc].

Römich et al. 2012 reported 85 xpT data points and the interaction parameters for [emim][OAc]-H_2O between a temperature range of 293.15 K to 353.15 K. Using the reported interaction parameters, the temperature dependency form shown in equations 4-3 to 4-6 was fitted for the data set. Employing the least

square as the equation error and the underlying assumptions stated earlier, the temperature-dependent NRTL parameters were optimized using the reported interaction energies. Table 2 presents the reported interaction parameters in Römich et al. 2012 and the optimized values determined as described above. (Römich et al., 2012)

$$G_{ij} = \exp(-\alpha_{ij}\tau_{ij}) \tag{4-3}$$

$$\tau_{ij} = \frac{\Delta g_{ij}}{RT} \tag{4-4}$$

$$\tau_{ij} = a_{ij} + \frac{b_{ij}}{T} + e_{ij}\ln T + f_{ij}T \tag{4-5}$$

$$\alpha_{ij} = c_{ij} + d_{ij}(T - 273.15) \tag{4-6}$$

Table 2: NRTL interaction parameters; water (1) and [emim][OAc] (2).

	Unit	12	21
Δg	J/mol	28938	-25691
a		7.15E-12	-3.9E-12
b		3480.64	-3090.09
c		0.1024	0.1024
d		0	0
e		-1.1E-12	6.14E-13
f		0	0

By way of verifying the accuracy of the fitted parameters, the experimentally measured bubble curves were charted together with the NRTL model prediction in Figure 10. The overall average relative error for the 85 data points calculated as $\frac{1}{N}\sum_i^N \left\{\left|\frac{P_{model}-P_{meas.}}{Pmeas.}\right| * 100\right\}$ is 5.47%.

Because of the low vapour pressure exhibited by ILs, it is customary not to show the dew point curves as the vapour phase almost entirely contains the volatile component; water in this case.

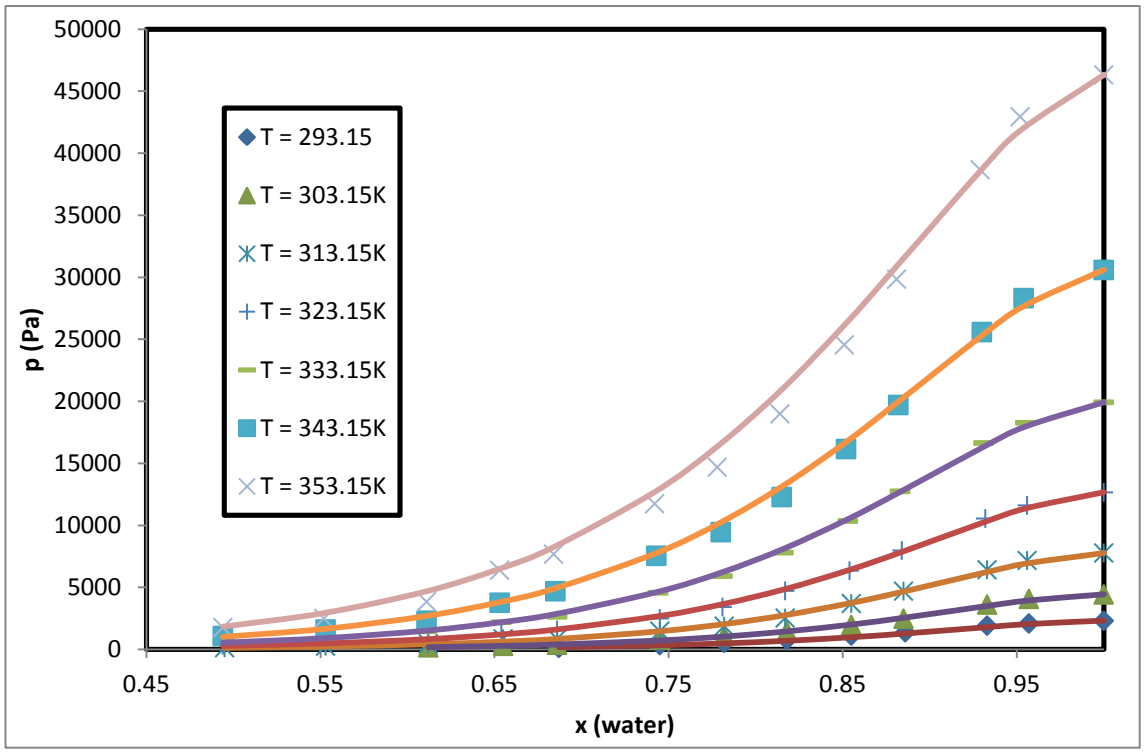

Figure 10: Comparation of experimental data with NTRL model prediction. The points and lines represent experiment data and model predictions respectively.

Some efforts were invested on modeling mixtures of [emim][OAc] and alcohols as well. These efforts were; however, hampered due to lack of experiment data to fit the Gibbs excess model parameters. The absence of the needed measured data in the literature demands the used of group contribution or the predictive models. Regarding the group contribution method, the present status of the UNIFAC main groups and subgroups is still limited in terms of ILs structure. Hector et al. 2013, Lei et al. 2008 and Nebig & Gmehling 2011 all contributed to extending the capability of UNIFAC model to handle ILs and alcohol mixtures. These efforts yielded new subgroups but the subgroups needed to capture

acetate and IL interaction are still missing. (Hector et al., 2013; Lei et al., 2012; Nebig and Gmehling, 2011)

Revelli et al. 2010 published some measured VLE data including that of 1-butyl-3-methylimidazolium acetate ([bmim][OAc])-methanol/ethanol mixture. Using these data alongside the water-[emim][OAc] reported in Römich et al. 2012, some new subgroups can be created with their interaction parameters optimized to handle mixtures of alcohol and the acetate-based ILs. Performing this kind of optimization is; however, beyond the scope of this thesis as it requires large amount of data and computer memory side by side with significantly robust algorithm.

4.2 Modelling of distillable and switchable ionic liquids

The task of VLE modelling distillable and switchable ionic liquids (DIL and SIL) is done together because of the similarity in the ILs chemistry. DILs are formed from organic base and acid; 1,1,3,3-tetramethylguanidine (TMG) is the commonly used base while any member of the alkanoic acid homologue can be the acid. Similarly, SILs are synthesized by reacting mixture of organic base and alcohol in the presence of a sour gas—either carbon dioxide or sulphur IV oxide. In this case, 1,8-Diazabicyclo[5.4.0]undec-7-ene (DBU) is a common based used for SIL synthesis.

Apart from being synthesized from molecular species, the formation of both DILs and SILs is also exothermic in nature. This exhibited exothermicity allows the regeneration of the starting molecular chemicals, which are employed to synthesize these ILs, by simple temperature increment. In essence, the chemical

equilibrium can be shifted in the desired direction by invoking thermal energy. The DIL and SIL considered in this modelling task have the following chemical pairs as their starting molecular species: TMG/propanoic acid for DIL and DBU/butanol/CO_2 for the SIL. Figures 11 and 12 depict the chemical equilibrium reaction between the ILs and their corresponding molecular conjugate.

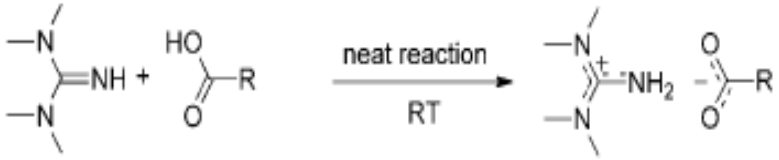

TMG + C_2H_5COOH ←----→ [TMGH][$C_2H_5CO_2$]

Figure 11: General scheme of DIL formation with TMG/propionic acid case.

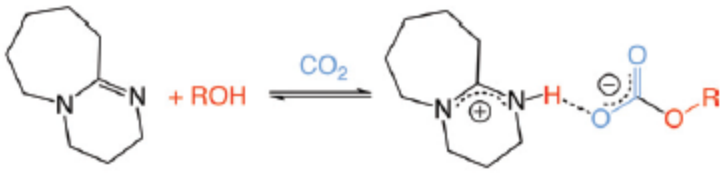

DBU + C_4H_9OH + CO_2 ←----→ [DBUH][$C_4H_9CO_3$]

Figure 12: General scheme of SIL formation with DBU/butanol/CO_2 case.

These choices of ILs were investigated because their biomass dissolution capability has been previously published (Anugwom et al., 2012; King et al., 2011). Moreover, there are some indirect data in the literatures from which their chemical equilibrium could be approximately modelled (Heldebrant et al., 2008; King et al., 2011). As mentioned earlier in subsection 3.1 of chapter 3, modelling chemical equilibrium involves total Gibbs free energy minimization for the system being considered. This minimization exercise can performed using either of the stoichiometric or non-stoichiometric approach.

In line with the stoichiometric approach, the total Gibbs free energy can be written in terms of the extent of reaction(s). The extent of reaction(s) that minimizes total Gibbs free energy dictates the equilibrium composition. Because the derivate of total Gibbs free energy with respect to reaction(s) extent at equilibrium is zero, the standard and excess parts of the total Gibbs free energy can be equated. This consequently allows reformulating the minimization problem as nonlinear simultaneous equations. Equations 4-7 to 4-10 present the nonlinear set of equations.

$$\Delta_r G^o = -RT \ln K_{eq} \tag{4-7}$$

$$K_{eq} = \prod (\gamma_i x_i)^{\nu_i} \tag{4-8}$$

$$\Delta_r G = \sum_i^n \nu_i \Delta_f G_i \tag{4-9}$$

$$\Delta_f G_i = \left(\Delta_f H_i^o + \int_{Tref}^{T} C_{p,i} dT\right) - T\left(\Delta_f S_i^o + \int_{Tref}^{T} \frac{C_{p,i}}{T} dT\right) \tag{4-10}$$

In order to model chemical and phase equilibrium (CPE) simultaneously, the phase equilibrium expression have to be solved alongside those of the chemical equilibrium. By way of reducing complexity, the CPE can also be handled by expressing the phase transitions as chemical equations and thus, maintaining the chemical equilibrium problem. The modelling tasks performed in this section consider only chemical equilibrium of the ILs and leaves the CPE treatment to the simulation section.

Starting with the SIL ([DBUH][$C_4H_9CO_3$]), the standard state enthalpy and Gibbs free energy of formation and the appropriate heat capacity correlation is needed for all the components. These data are available in common physical

properties databases for carbon dioxide and butanol but not for DBU and the SIL. Three different group contribution methods were used to estimate the standard state enthalpy and Gibbs free energy of DBU as ideal gas; the Joback method and two other methods developed for biological systems by Mavrovouniotis 1991 and Jankowski et al. 2008 (Jankowski et al., 2008; Mavrovouniotis, 1990; Poling et al., 2001). The other two methods asides Joback were employed because the nitrogen ring group (—N<) is absent in the Joback group table, hence, the aliphatic equivalent was employed for the estimation. Table 3 presents the result of the estimations.

Table 3: Thermodynamics properties of DBU from group contribution methods.

		$\Delta_f H^o$	$\Delta_f G^o$
		kJ/mol	kJ/mol
Joback method		79.18	321.6
Jankowski et al. 2008		-	245.6
Mavrovouniotis 1991		-	397.1

Additionally, the heat capacity as ideal gas was estimated with Flowbat—the in-house process simulator developed in Aalto University—using the Harris and Seaton's property estimation method. As for the SIL, there are currently no estimating methods for them. Heldebrant et al. 2008, however, reported enthalpy, entropy and Gibbs free energy data for eighteen different CO_2 capturing reactions forming different SILs at 1atm and 25 degree Celsius. These data include that of the SIL considered, thus, the standard state thermodynamics properties of the SIL in liquid state was back-calculated. In this calculation, the ideal gas standard state properties for DBU were converted to liquid state using the enthalpy of vaporization, also estimated with Flowbat, while the liquid state properties of butanol was collected the DIPPR 801 project

book. Table 4 presents reaction data from Heldebrant et al. 2008 and the calculated values for the SIL.

Table 4: Reaction data and estimated properties for SIL.

$\Delta_r H$	$\Delta_r G$	$\Delta_r S$
kJ/mol	kJ/mol	kJ/(mol-K)
-140	-9.7	-0.45
		SIL, liquid
$\Delta_f H^o$	kJ/mol	-844.9
$\Delta_f G^o$	kJ/mol	-137.2
$\Delta_f S^o$	kJ/(mol-K)	-2.16

In addition to this, the equilibrium constant is estimated with the reported Gibbs energy of reaction and then extended with the van't Hoff equation, which extends chemical equilibrium constant as a function of temperature assuming a constant enthalpy of reaction. With the extended value of equilibrium constant, the heat capacity of the SIL was optimized using equations (4-7), (4-9) and (4-10). The liquid state heat capacity of DBU was calculated by backward difference method using the liquid state enthalpies calculated from the previously estimated ideal gas heat capacity and the Watson's extension of the enthalpy of vaporization.

The optimization of the heat capacity of the SIL could not be easily converged due to the nonlinear nature of the equations employed. Hence, a linear equation (4-11) relating equilibrium constant and change in heat capacity parameters was employed (Smith and Van Ness, 1987).

$$\ln K_{eq} = \frac{-J}{RT} + \Delta A \ln T + \frac{\Delta B}{2} T + \frac{\Delta C}{6} T^2 + \frac{\Delta D}{2T^2} + I \qquad (4\text{-}11)$$

The least square optimized parameters for equation (4-11) was then used to determine the SIL liquid state heat capacity correlation coefficients. The calculated coefficients were validated by calculating the heat capacity at 300K; the determined value—1.73 J/(g-K)—at least passed the test of 1.2 to 2 J/(g-K) range predicted by Heldebrant et al. 2008. Figure 13 compares the van't Hoff-extended equilibrium constant with the modelled values based on equation (4-11) optimization. A similar graph was obtained when the determined SIL heat capacity was transferred to the nonlinear model.

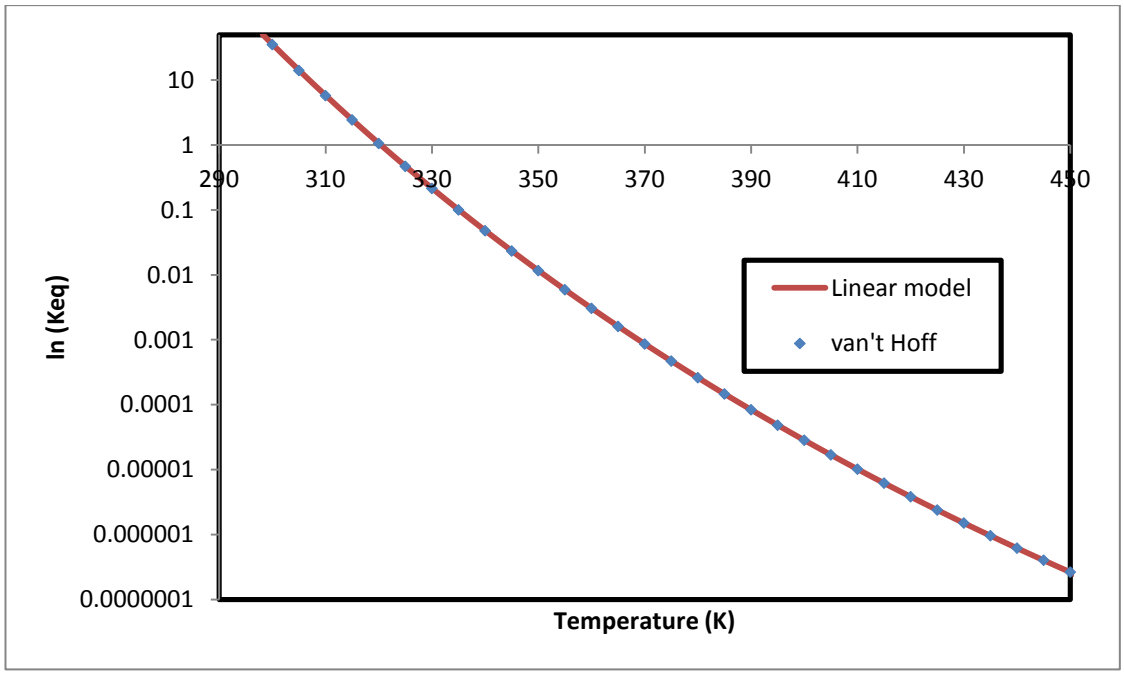

Figure 13: Chemical equilibrium constant comparation.

In the case of the DIL ([TMGH][$C_2H_5CO_2$]), the thermogravimetric analysis (TGA) graph that is reported in King et al. 2011 was traced for the dissociation profile of the DIL with respect to temperature. Using these data and the known

stoichiometric reaction of the dissociation—shown in Figure 11—, the corresponding amounts of propionic acid and TMG were calculated. Consequently, the reaction equilibrium constant was estimated for the temperature range with equation (4-8). The activity coefficients were assumed to be unity throughout this calculation. It is possible to use UNIFAC method for the TMG-propionic acid interaction parameters but this method is not matured enough for the IL interaction computation.

Just like in the case of the SIL, the liquid state thermodynamics data for propionic acid were collected from the DIPPR 801 project while that of TMG was calculated from the ideal gas estimation using Aspen property estimation. Flowbat was also used for TMG property estimations for validation purpose, both software programs; however, yield similar values. Similarly, equation (4-11) was used to fit the DIL heat capacity but this time, equations (4-7) to (4-10) were utilized to optimize the DIL standard state enthalpy and Gibbs free energy. Figures 14 and 15 illustrate how the TGA-traced values compare with the linear and nonlinear models optimization respectively.

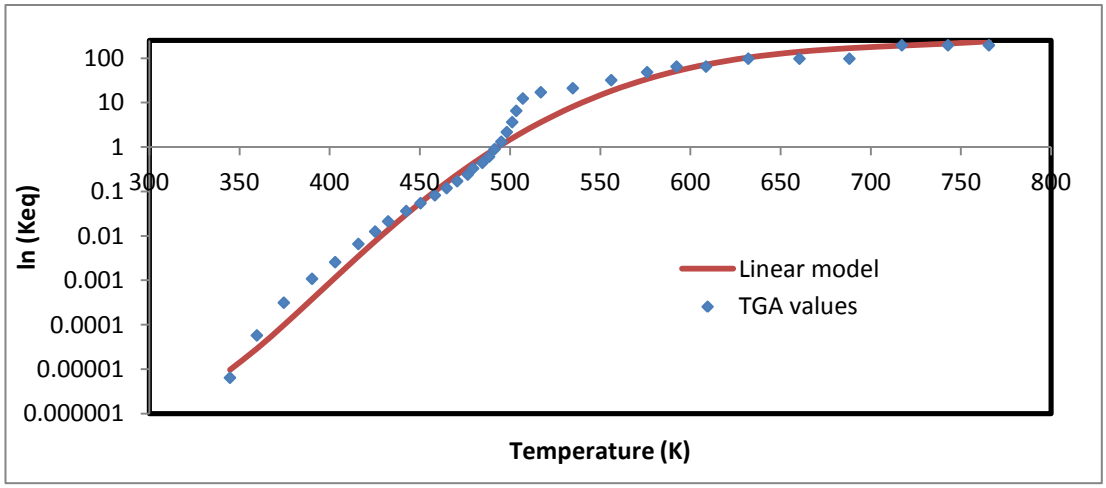

Figure 14: Equilibrium constant of the DIL against temperature; linear optimization.

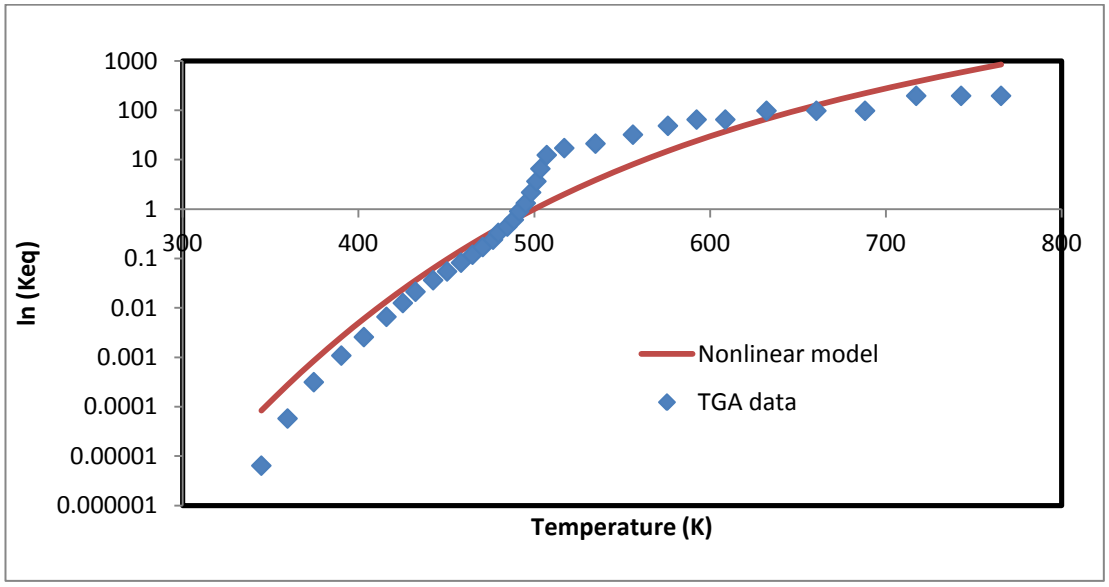

Figure 15: Equilibrium constant the DIL against temperature; nonlinear optimization.

The irregularities shown in the TGA values indicate some level of human error in the process of data tracing. Additionally, this error makes it difficult for the models to perfectly fit the data. The encountered imperfection is; however, immaterial as only a rough estimation is needed to carry out the simulation.

As a closure to this chapter, the main achievements are briefly recounted as follows. Firstly, the platform for calculating the VLE and CPE of the ILs was established. Furthermore, the physical properties of the ILs needed in thermal separation calculations were also estimated. These physical properties are either calculated with the group contribution methods or by indirect optimization of model parameters. Appendix D presents the results of the intermediate calculation results that are not included within the chapters.

5 Process Simulations of Separation and Recycling Schemes

Chapter 4 effectively dealt with the VLE and chemical equilibrium modelling (CE) of the ILs types in consideration. In this chapter, the results from the VLE and CE modelling shall be harnessed to simulate possible separation and recycling schemes for the ILs-antisolvent mixtures. Just like in chapter 4, the first and second sections shall consider the imidazolium-based ILs and the DIL/SIL respectively.

5.1 Separation and recycling schemes for imidazolium-based ILs

The goal of this section is to report the procedure and results of the biomass fractionation process simulation with [emim][OAc] as IL and water as antisolvent. The motivation behind this choice of IL/antisolvent was explained in heading 4.1 of chapter 4. This simulation was performed with Aspen Plus software V7.3 with some physical properties data supplied from external calculations and correlations parameter fitting.

Based on the biomass fractionation description given in chapter 2, the general flowsheet consist of the fractionating section and the thermal separation parts. Figure 16 illustrates the general layout of the six unit operations used for the process simulation. In the first tank, the employed IL would fractionate biomass; whether cellulose, hemicellulose or lignin is fractionated depends on the IL employed. The second block separates the undissolved biomass from the IL-dissolved biomass stream. The next block, mixer, depicts the precipitation of

the dissolved biomass fraction with an antisolvent. Following the precipitation is the filtration of the precipitates and subsequent thermal separation of the IL-antisolvent mixture.

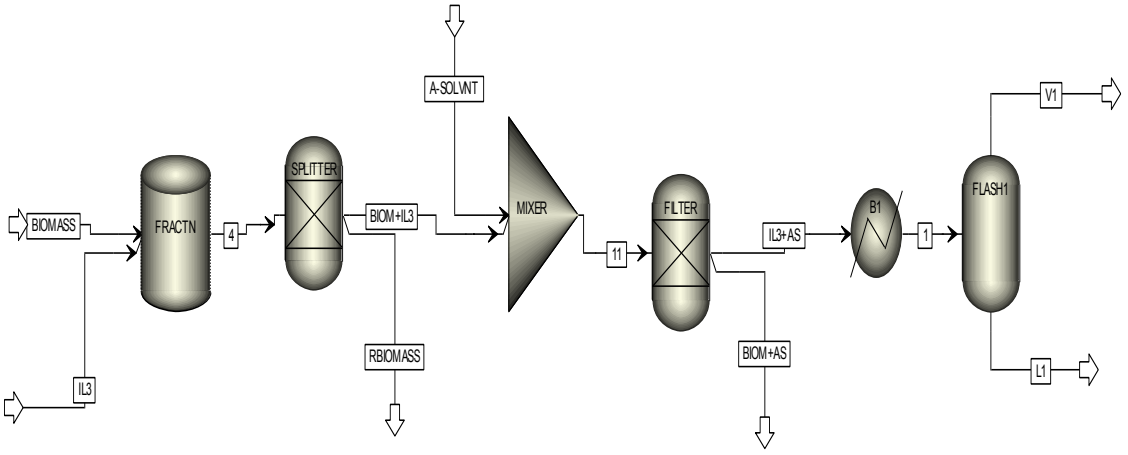

Figure 16: Illustration of biomass fractionation process layout.

In all the simulations reported, the fractionation and precipitation parts are simply modelled with splitters and mixers while the thermal separation part is rigorously modelled with the specified thermodynamic models. Accurately modelling biomass fractionation and precipitation demands the definition of biomass as non-conventional solid. Furthermore, reactor models like the Gibbs reactor or a kinetic reactor model would be required. In order to capture the phenomenon of interest, dissolution and precipitation, these reactor models would require thermodynamics and kinetics data which are presently unavailable in the literature. As such, the aforementioned approach with specified split ration was used as the focus of the simulation is on the separation and recycling parts.

In consistent with reported laboratory experiments, the feed ratio of IL to biomass is chosen to be greater than unity; that is 80 kg/s IL and 20 kg/s biomass (Anugwom et al., 2012; Kilpeläinen et al., 2007; van Spronsen et al., 2011). Furthermore, an antisolvent feed of 100 kg/s was introduced for precipitating the dissolved biomass. Biomass split ratio of 50% was specified for the outlets in the second block (splitter) to model 50% dissolution of biomass while a total removal of the supposedly dissolved biomass was imposed in the forth block (filter) to demonstrate filtration of the precipitate. In the blocks labelled 'SPLITTER' and 'FILTER', little amount of IL and IL-antisolvent mixture was specified as loss to the outlet streams in both cases.

Because the IL ([emim][OAc]) is a non-database component, it is modelled as pseudocomponent with its molecular mass, normal boiling point, density, vapour pressure and critical properties specified. The normal boiling point, density and critical properties of [emim][OAc] are estimated based on the modified Lydersen-Joback-Reid method for ILs developed by Valderrama & Rojas 2009. (Valderrama and Rojas, 2009)

Additionally, data for estimating the energy variables are supplied for [emim][OAc]. Römich et al. 2012 reported some specific heat capacity data for [emim][OAc]-water mixture for a temperature range of 293.15K to 363.15K. These data were extrapolated to calculate the specific heat capacities of pure [emim][OAc] at the reported temperatures. The extrapolated values were compared with specific heat capacities calculated from an additive method reported in Soriano et al. 2010 and both estimates show considerable agreement. Enthalpy of vaporization at 298K was estimated from a predictive rule given in Verevkin et al. 2008 and extended with Watson correlation for other

temperatures. All the mentioned data were fitted to the Aspen Plus correlations and the parameters were supplied for the simulations. Equations 5-1&2 and Tables 5 and 6 show the correlation of specific heat capacity and the fitted parameters estimated as earlier described. (Soriano et al., 2010; Verevkin, 2008)

$$C_p^{IG} = C_1 + C_2T + C_3T^2 + C_4T^3 + C_5T^4 + C_6T^5 \quad C_7 \le T \le C_8 \qquad (5\text{-}1)$$

$$\Delta H_{vap}(T_2) = \Delta H_{vap}(T_1)\left(\frac{1-\frac{T_2}{T_C}}{1-\frac{T_1}{T_C}}\right)^{a+b\left(1-T/T_d\right)} \qquad (5\text{-}2)$$

Table 5: Estimated parameters for specific heat capacity of [emim][OAc]

C_p^{IG} (kJ/kmol-K)		ΔH_{vap} (kJ/mol-K)	
C1	27278.19	$\Delta H_{vap}(T_1)$	119.8
C2	-337.76	T (1) (K)	298
C3	1.5776	a	0.38
C4	-0.0033	b	0
C5	2.5375E-06	Tmin (K)	298
C6	0		
C7	302		
C8	600		

Table 6: Specific heat capacities comparation

	T	C_p^L (extrapolated)	C_p^L (predictive)
UNITS	K	J/(mol-K)	J/(mol-K)
	293.15	310.66	324.06
	303.15	314.33	326.92
	313.15	315.83	330.37
	323.15	319.81	334.42
	333.15	323.72	339.06
	343.15	325.78	344.30
	353.15	330.11	350.13
	363.15	337.58	356.55

Biomass is modelled as cellulose and the remaining components are normally chosen from the database. Asides from the supplied data stated above, the remaining physical properties needed within the simulation were estimated by Aspen Plus inbuilt methods.

Having set up the simulation platform, the first simulation is run with ideal model assumptions to realize the level of nonideality exhibited by the system. Following the ideal simulation, a nonideal case was also simulated with the NRTL model and all the fitted energy variables data. The normal boiling point rise of water due to the presence of [emim][OAc] is also investigated.

Figure 17 shows a schematic of the single flash separation of the IL-antisolvent mixture. Following the set-up in Ferro et al. 2012, the IL-water mixed stream to be separated is heated to its bubble point before flashing so as to distinguish the sensible heat and from the heat required for vaporizing the mixture. In order to ensure that [emim][OAc] does not decompose, a ceiling temperature of 400 K is specified in the flash drum. (Ferro et al., 2012)

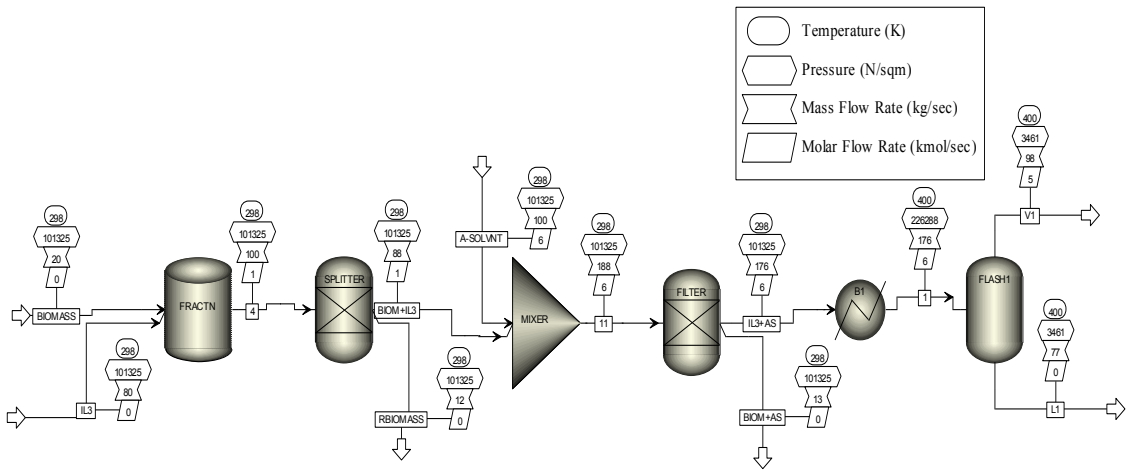

Figure 17: Single flash separation of [emim][OAc]-water mixture.

Table 7 compares the results from the single flash separations; the results from the ideal and nonideal simulations were compared. Apparently, due to the low vapour pressure exhibited by the [emim][OAc], flashing the liquid mixture in a single drum attains a reasonable level of purity. However, the specified temperature (400 K) demands operating in vacuum to achieve the separation; the ideal case requires about 3.5 kPa while the data-supported case went as low as 0.33 kPa. The attained level of purity and the required energy are comparable while the normal boiling point rise of the data-supported case more than doubles that of the ideal simulation.

Table 7: Ideal and data-supported single-stage flashing.

		IDEAL	DATA-SUPPORTED
Temperature	K	400	400
Pressure	Pa	3461	328
SEPARATION	%wt IL in Vapour	0.005	0.043
	%wt IL in Liquid	0.999	0.993
ENERGY	Qheat MW	34.46	9.14
	Qheat kJ/kg IL	443.94	117.72
	Qvap MW	214.72	242.84
	Qvap kJ/kg IL	2766.40	3128.78
	Qtotal MW	249.18	251.98
DTBR		2	5

Furthermore, an exponential increase in boiling point rise of water is observed as the weight percent of [emim][OAc] grows in the mixture. Conversely, the total pressure of the IL-water mixtures reduces with amount of IL increases. Figure 18 depicts the observed boiling point temperature-rise trend in a semilog

graph while Figure 19 presents the bubble temperature and pressure of the mixture over some composition range. Figure 19 is in essence a design chart from which the required tank pressure can be determined based on the operating temperature and the desired purity.

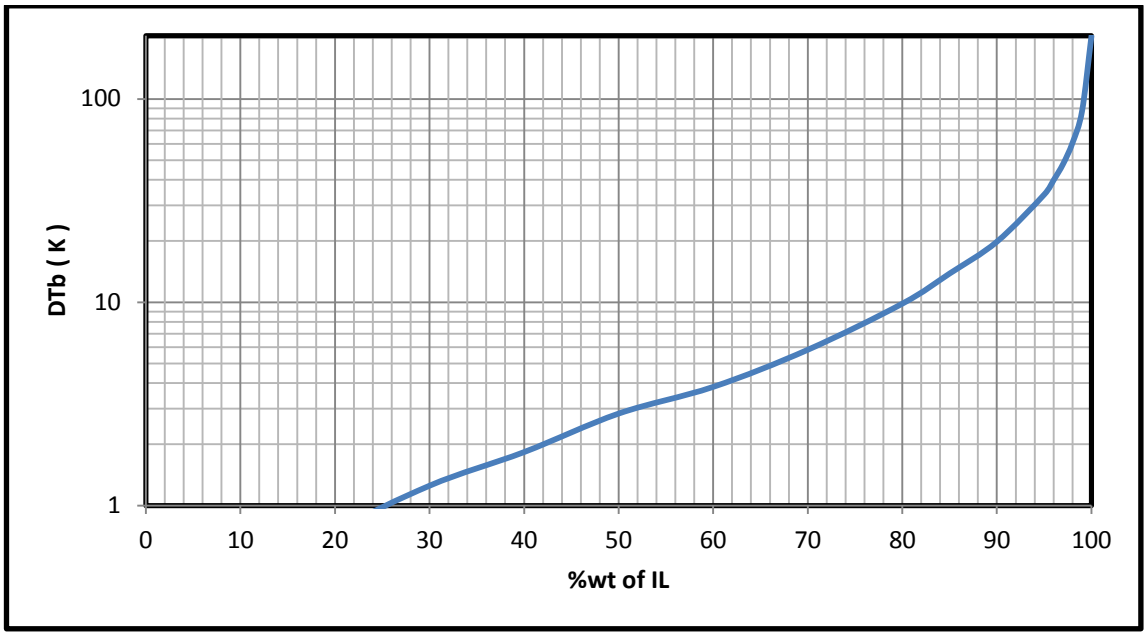

Figure 18: Semilog plot of boiling point rise of water at 1 atmosphere.

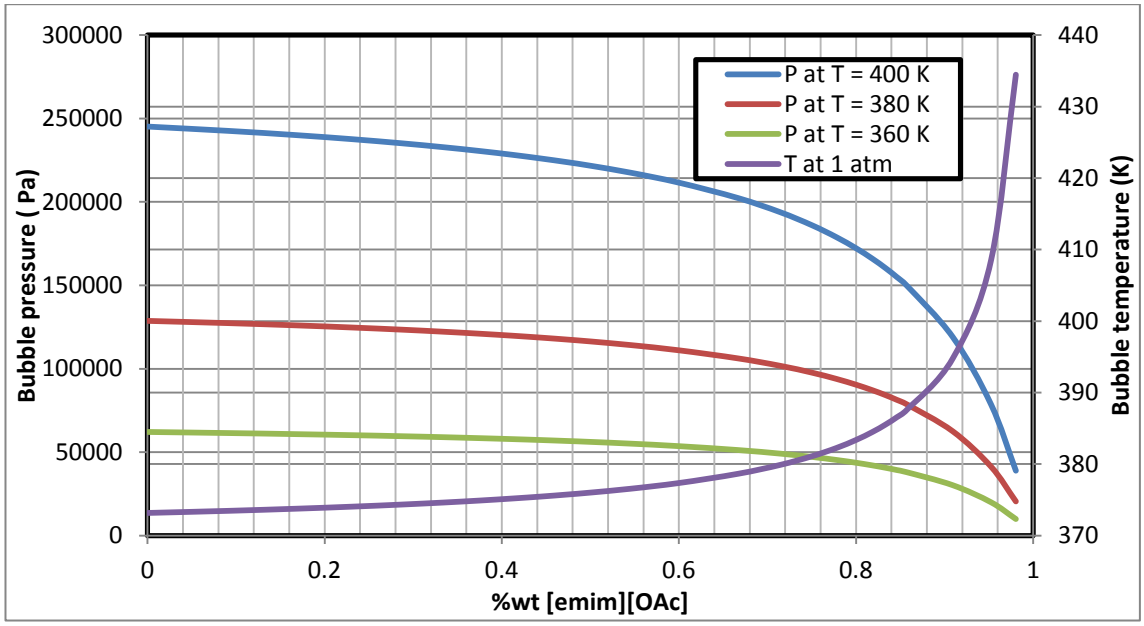

Figure 19: Bubble pressure and temperature against % weight of [emim][OAc].

Lastly, for the sake of energy economy, an optimized three-stage flash with a recycle stream is simulated for the biomass fraction process. As shown in Figure 20, the vapours from the first and second stages were condensed to flash the content of the second and third drums sequentially. Hence, the only energy input goes to the first flash tank. In order to minimize the energy consumed in the first tank, the optimization tool in Aspen Plus is set up as follows;

Objective function → $Minimize\ \ Q1$ (Energy consumed in the 1st flash tank)

Optimized variable → $\left(\frac{V}{F}\right)_{TANK1}$ (Vapour to feed ratio in the first flash tank).

Constraints → $x_{[emim][OAc]} = 0.95$ (Mole fraction of IL in stream 6)

$$T_1 - T_2 \geq 10\ K$$
$$T_2 - T_3 \geq 10\ K$$
$$P_1 \leq 200\ kPa$$
$$P_1 \geq 100\ kPa$$
$$P_2 \leq 200\ kPa$$
$$P_2 \geq 100\ kPa$$

The first constraint represents the purity level required in stream 6—the recycle stream— as shown in Figure 20. T_1, T_2 and T_3 denote the temperatures in the evaporator stages. The temperature differences demand in the constraint equations are needed to ensure the usability of the condensed vapours in the subsequent stage. Lastly, the dictated pressure window in tanks 1 and 2 are chosen to ensure easy operation of the flash tanks around atmospheric condition.

Table 8 presents the results obtained from the converged simulation. 99.2 weight percent of [emim][OAc], corresponding to 93.3 mol percent, was realized in the recycle stream and the pressure level in the third tank was at 2 kPa to achieve this purity. Temperature difference between flash tanks 1-2 and 2-3 is 10 K and 30 K respectively while the energy input is more than halved as compared to the single flash tank case. The observed large temperature difference between flash tanks 2 and 3 at the optimum condition allowed for effective usage the energy transfer. This temperature difference together with flash tank 3 pressure of 2 kPa provided the driving force needed to effectively concentrate the viscous IL-water mixture to the specified concentration.

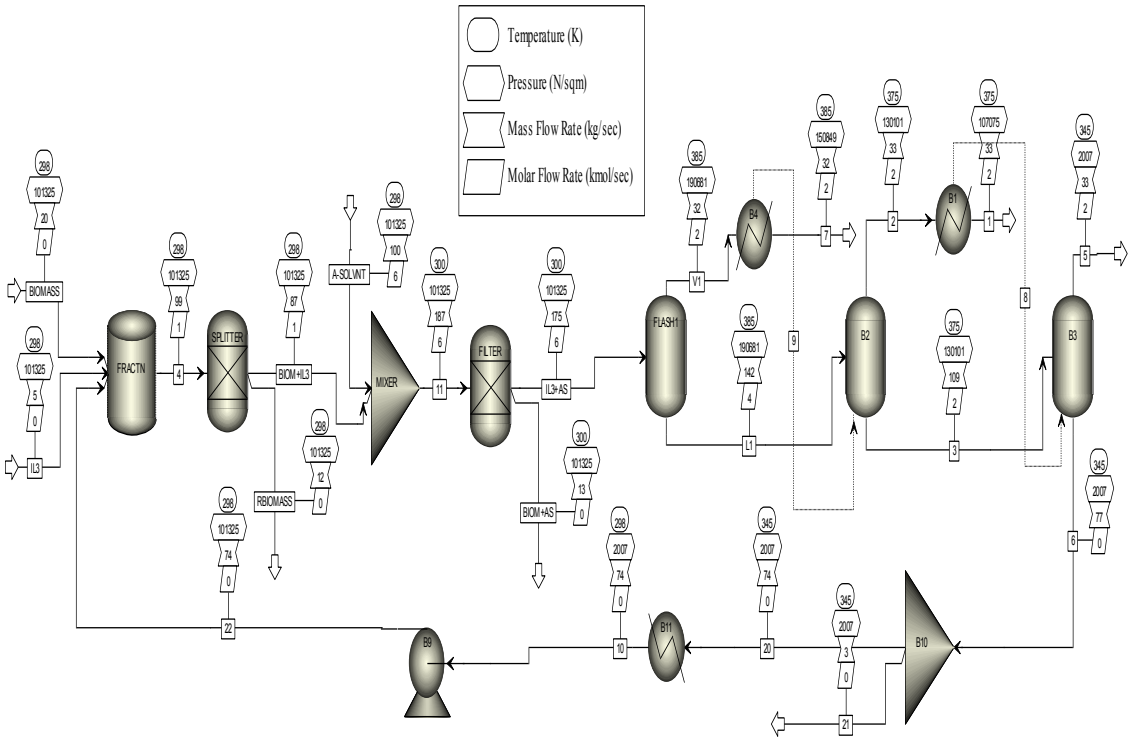

Figure 20: Optimized three-stage flash with recycle.

Table 8: Results from single and multistage separation.

		MULTIFLASH (*optimized)*	SINGLE FLASH
Temperature	K	(385,375,345)	400
Pressure	kPa	(191; 130; 2)	0.328
SEPARATION	%wt IL in Vapour	11 ppm	0.043
	%wt IL in Liquid	0.99	0.99
V/F ratio		(0.3; -; -)	0.92
ENERGY	Qflash MW	112	251

5.2 Separation and recycling schemes for DILs and SILs

The general biomass fractionation flowsheet described in section 5.1 is exactly the same in this section except for the employed IL. For both ILs, carbon dioxide, butanol, TMG, and propionic acid are all Aspen Plus database component. Water and cellulose were used as the antisolvent and biomass respectively. The molecular structure of TMG is drawn in the mol-file for group contribution estimation of the missing properties. Likewise, the structure of DBU was drawn for possible properties estimations; however, as the nitrogen ring (-N<) subgroup is not available in many group contributions methods, the properties that could not be estimated were calculated in Excel using the non-ring equivalent. The estimated values were then supplied into Aspen for simulation purpose.

Both the SIL and DIL were modelled as pseudocomponents with the molecular weight, normal boiling temperature, density and vapour pressure data supplied to Aspen Plus. The critical properties, density and normal boiling point of the ILs were estimated with the modified Lydersen-Joback-Reid method developed by Valderrama & Rojas 2009. The vapour pressure of the ILs and that of DBU was estimated with the Riedel correlation in Flowbat. Figure 21 compares the vapour pressure of both ILs.

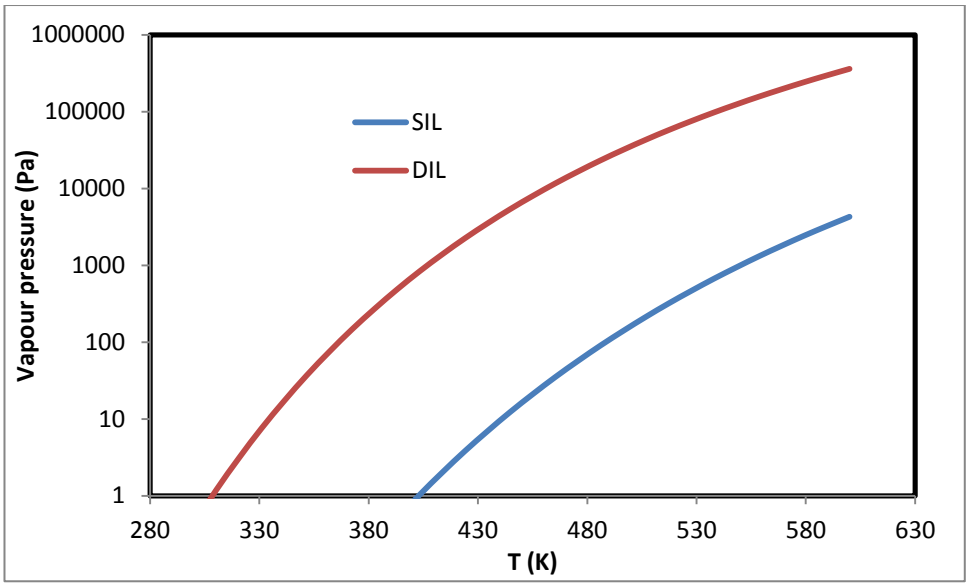

Figure 21: Semilog plot of ILs vapour pressure.

The enthalpy of vaporization for the ILs was estimated with the predictive method in Verevkin et al. 2008 and extended with Watson correlation. The Joback method is used to estimate all physical properties needed for DBU except for the ideal gas heat capacity that was calculated with Harris and Seaton's property estimation method. Using the optimized values for the ILs standard state enthalpy of formation, Gibbs free energy and heat capacity as liquid described in section 5.1, the standard state equivalents as ideal gas were back-calculated by setting the reference temperature at 298.15 K. Lastly, the equilibrium constant was fitted to equation (5-3) and the obtained values are

shown in Table 9. All the estimated values were fed into Aspen Plus for the flowsheet simulation.

$$\ln K_{eq} = A + \frac{B}{T} + C \ln T + DT \qquad (5\text{-}3)$$

Table 9: ILs equilibrium constant coefficients.

	SIL	DIL
A	-52.57	-1182.30
B	16839.07	29617.32
C	-4.41E-13	199.03
D	0	-0.23

Having estimated the needed physical properties, the flowsheet was set up just as in the case of imidazolium IL—[emim][OAc]. The ILs feed (80 kg/s) and the splitters specifications were similar to the case of [emim][OAc] for the purpose of later comparation. After the fractionation and precipitating section, the stream to be separated and recycled contains the IL (SIL or DIL) and the antisolvent (water). In accordance with the easy distillability of the ILs, the idea is to switch the ILs to their molecular conjugates and then separate the components. Switching and separating the components requires a reactive unit alongside a thermal separation process. In light of these facts, some separation and recycling schemes were developed for the ILs in questions.

Starting with the DIL, the first scheme (Figure 22) simulated takes advantage of the traditional ILs low vapour pressure. A simple vacuum distillation was employed to separate water from the DIL-water mixture and then recycling the DIL-rich stream. In order to get the desired purity—0.999 mol% of water— at the distillate, the column was operated with a total of 15 stages, 1.5 reflux ratio

and 5.3 kPa. The reboiler and condenser temperature are 445 and 307 K respectively. This magnitude of condenser temperature suggests the feasibility of employing cooling water as the coolant and thus neglecting the cost of cooling. Figures 23 to 25 show the separation and temperature profile of the column.

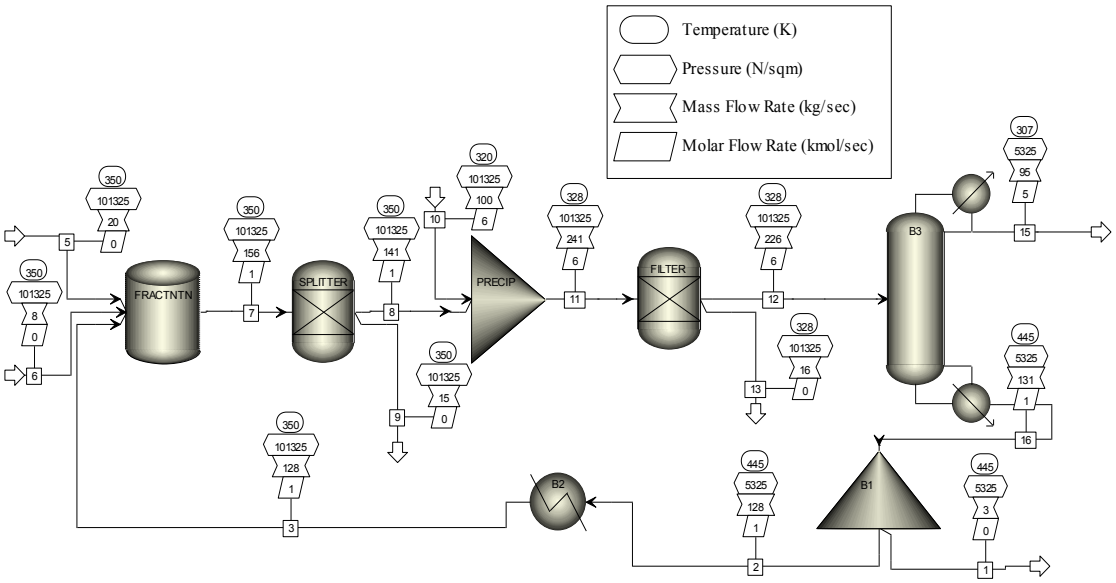

Figure 22: DIL-mixture purification and recycling scheme; CASE 1.

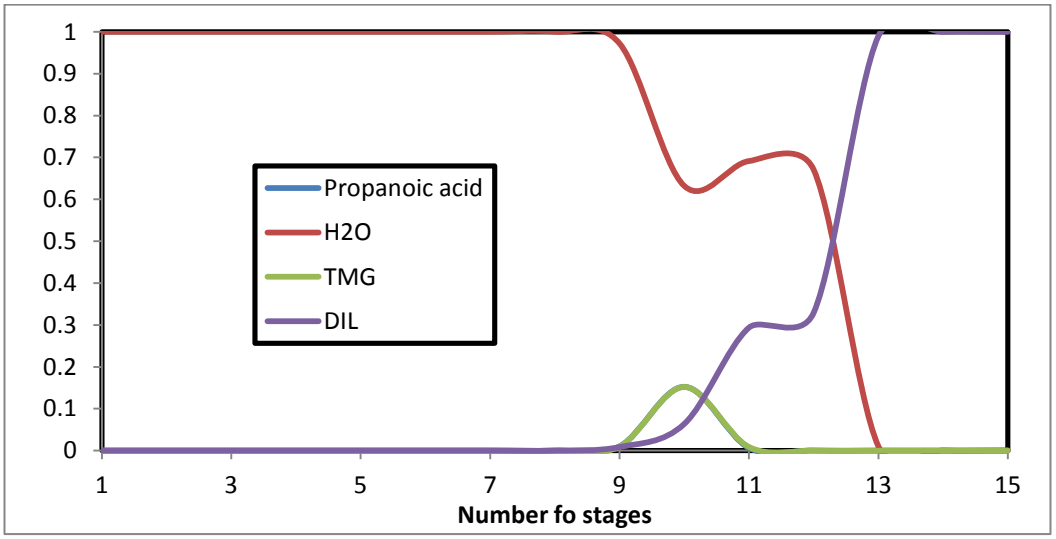

Figure 23: Vapour phase component profile. Stage 1 is the condenser.

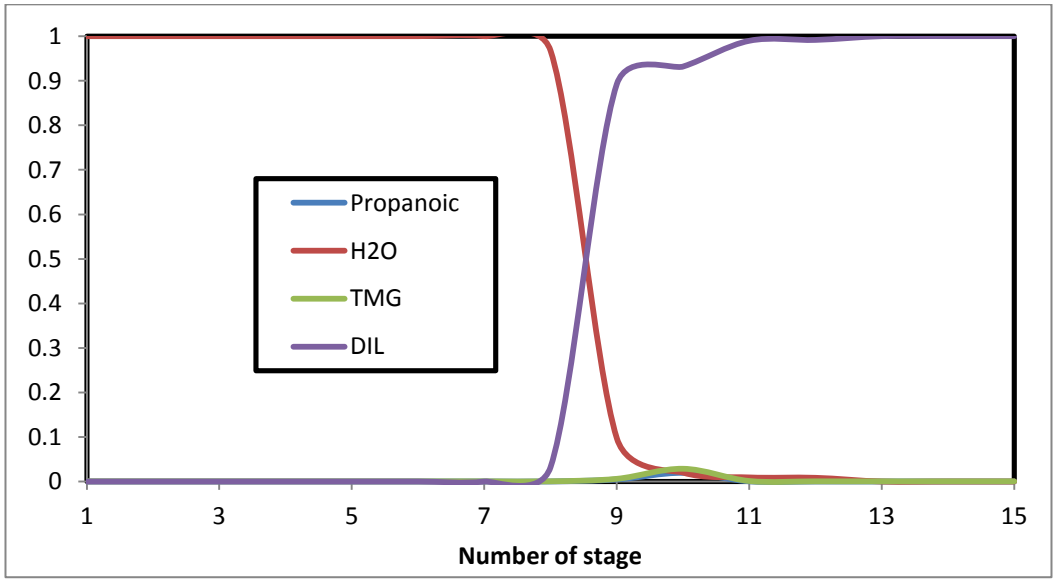

Figure 24: Liquid phase component profile. Stage 1 is the condenser.

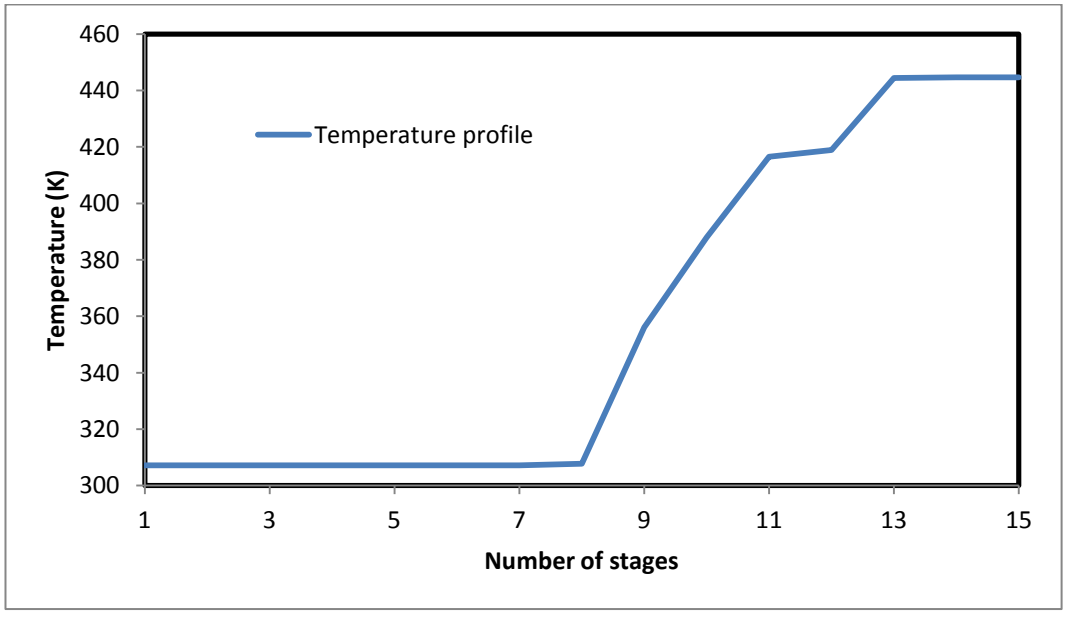

Figure 25: Temperature profile of the 15-stage distillation column.

The second scheme—CASE 2—simulated passes the DIL-water mixture through a CSTR reactor to switch-off the IL. The IL switching-off in the CSTR was calculated based on the equilibrium constant model (equation 5-3) and not kinetically. Complete switching off the DIL was achieved with a residence time and reacting temperature of 20 seconds and 450 K respectively. The CSTR outbound multicomponent stream, TMG, propionic acid and water, has the water content vapourized in a 15-stage column operated at 1 atm. Again, purity level of 0.99 mol% water was achieved and the TMG-propionic containing stream was led into another CSTR for their eventual switching-on to synthesize the recycled DIL. In this case, the CSTR was operated at 350 K to favour equilibrium shift in the direction of DIL. Figure 26 depicts CASE 2 scheme flowsheet. Figure 27 and 29 also depicts the distillation column vapour/liquid compositions and the temperature profile.

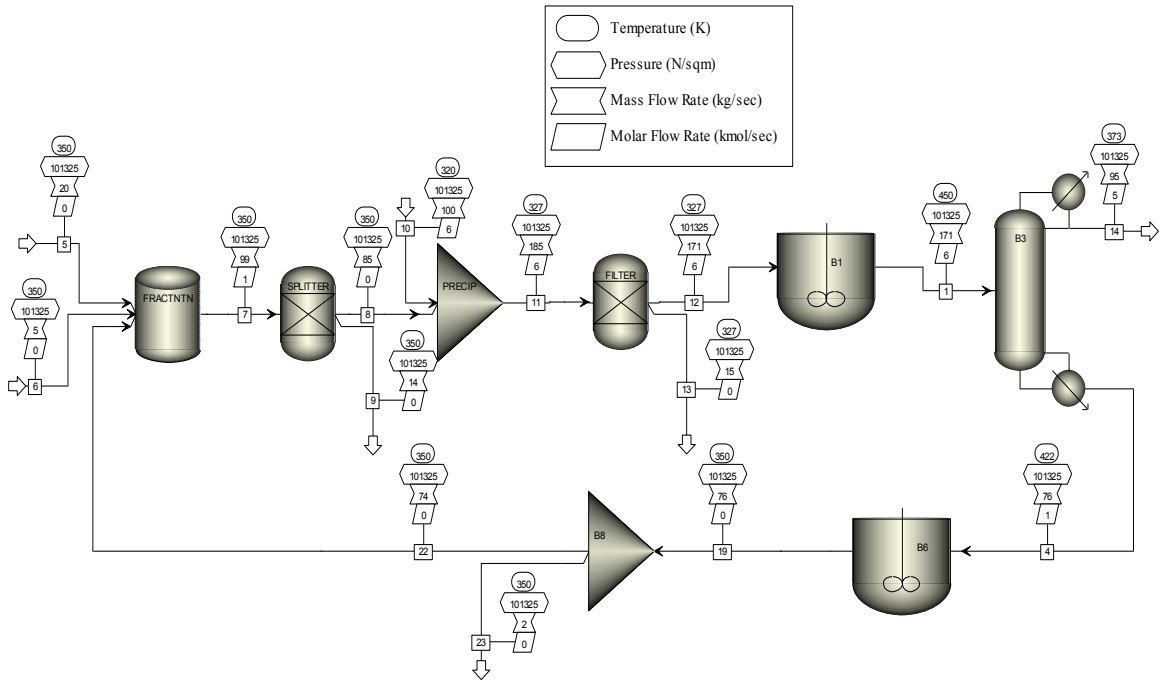

Figure 26: DIL-mixture purification and recycling scheme; CASE 2.

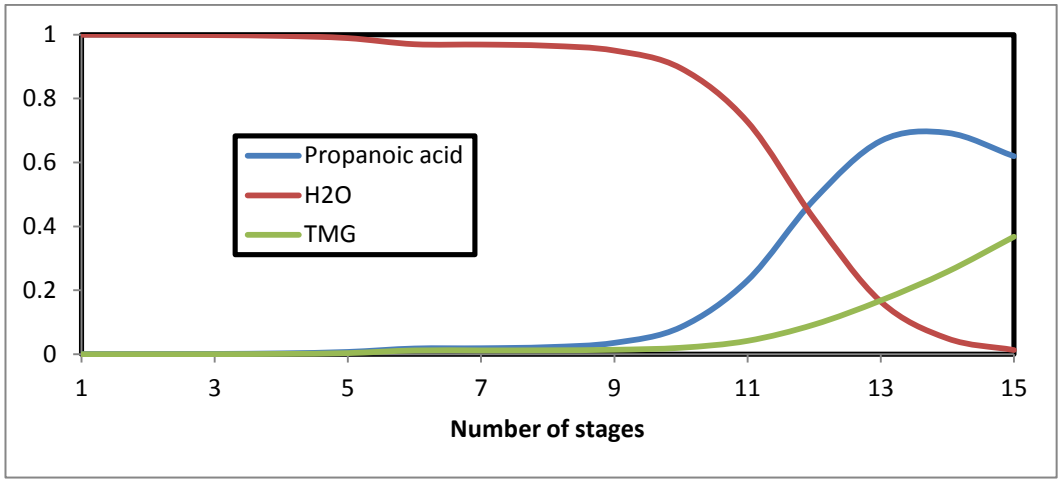

Figure 27: Vapour phase composition profile. Stage 1 is the condenser.

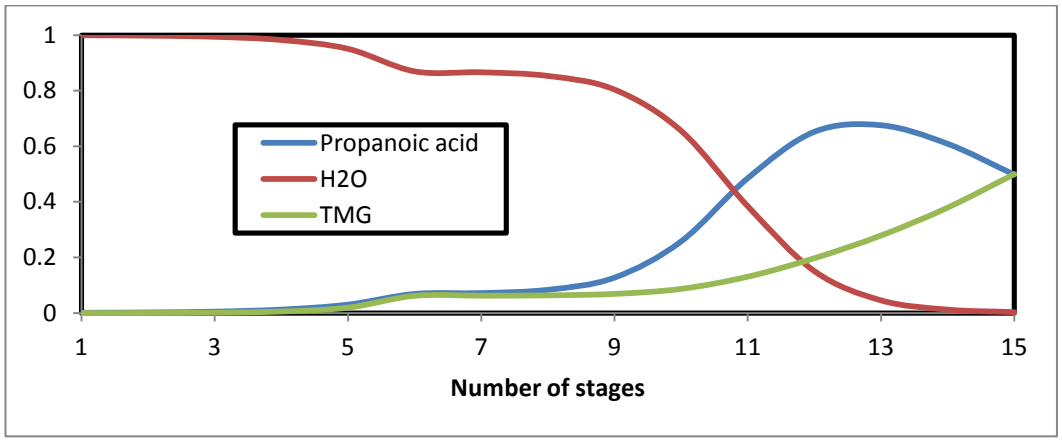

Figure 28: Liquid phase composition profile. Stage 1 is the condenser.

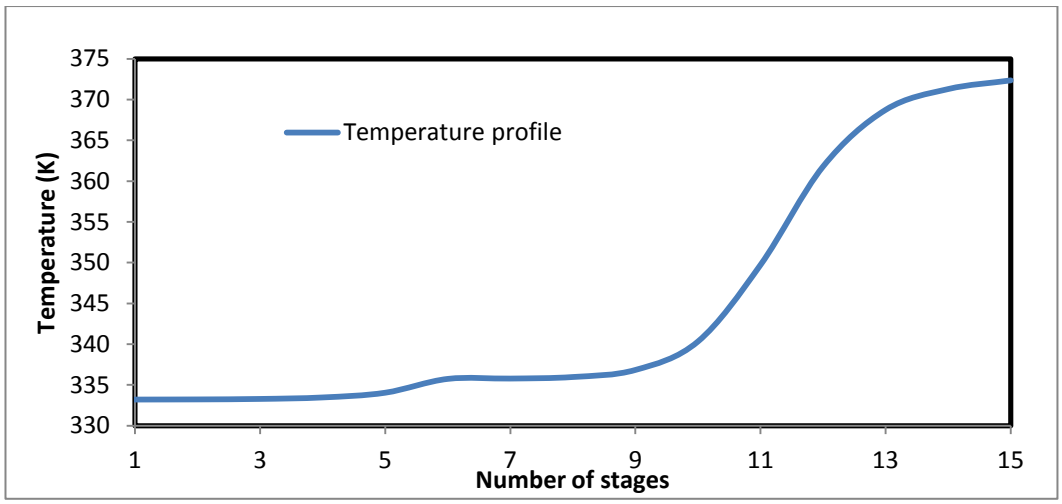

Figure 29: Temperature profile of the 15-stage distillation column (1 atm).

Following the DIL simulation, the SIL case was considered. As the molecular components of the SIL involve a gaseous component, the multicomponent separation is more complex for this IL. Figure 30 illustrates the simulated flowsheet.

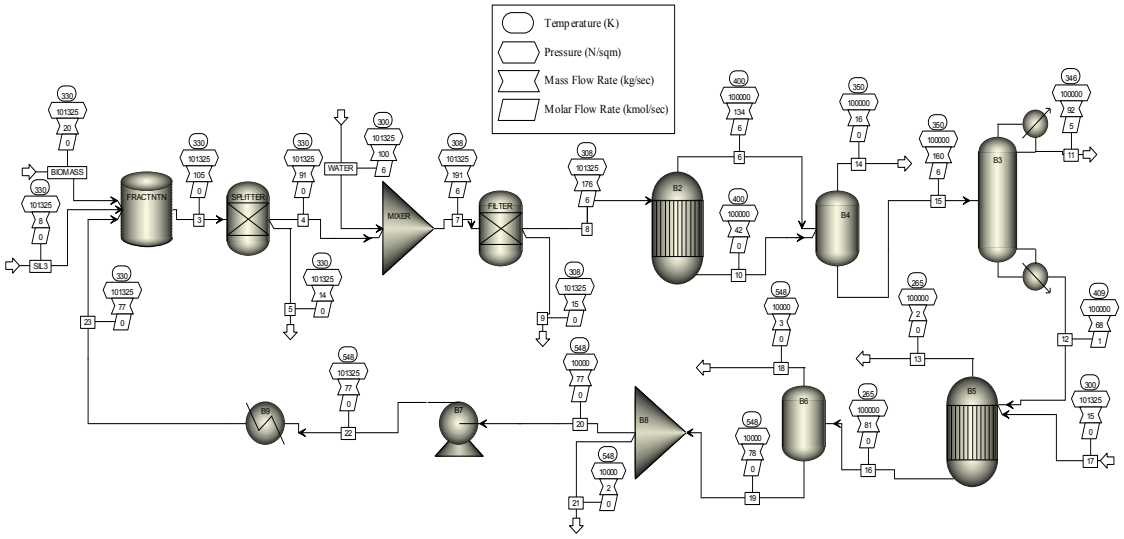

Figure 30: SIL-mixture purification and recycling scheme.

Because of the experimental data collected from Helderant et al. 2008, the thermodynamics data fed to Aspen Plus were more reliable, and thus, the chemical equilibrium can be accurately calculated from the first principle. In light of this fact, the stoichiometric equilibrium reactor was employed for the switching-on/off of the SIL. The scheme for the SIL is similar to CASE 2 of DIL save for the usage of two extra flash drums for partially separation of the CO_2. After switching off and partly vaporizing the CO_2 content of the multicomponent mixture, the distillation column removes the water and remaining CO_2. Consequently, the SIL is re-synthesized, purified and recycled as illustrated in the flowsheet.

Figures 31 to 33 show the composition and temperature profiles of the 50-stage column that separates water and CO_2. The high number of stages required for the separation reflects the closeness the boiling point of butanol and water.

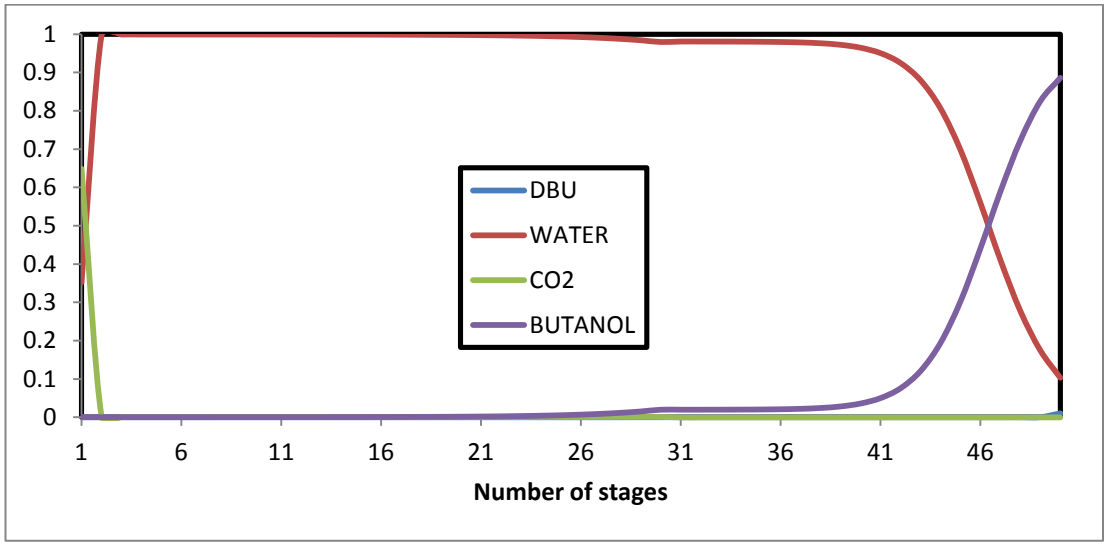

Figure 31: Vapour phase composition profile. Stage 1 is the condenser.

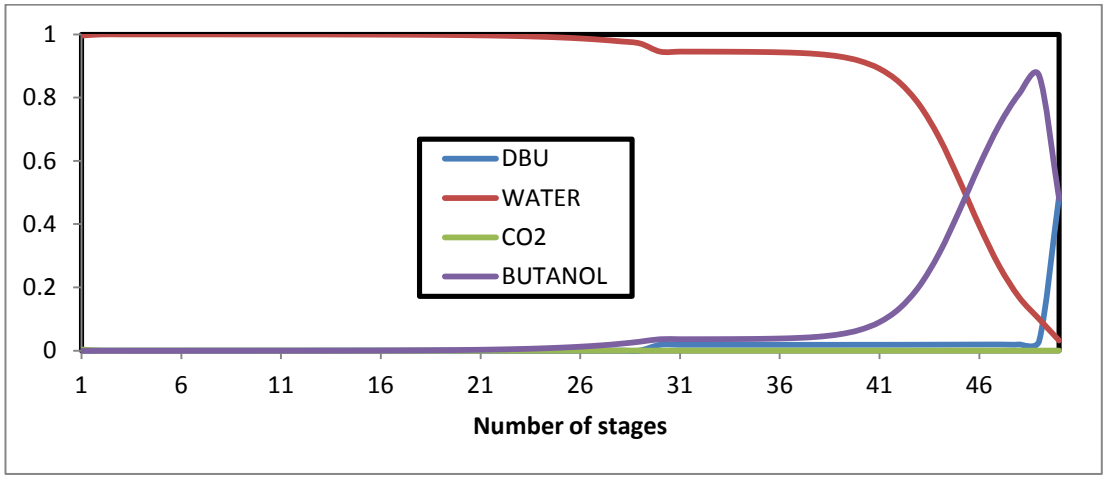

Figure 32: Liquid phase composition profile. Stage 1 is the condenser.

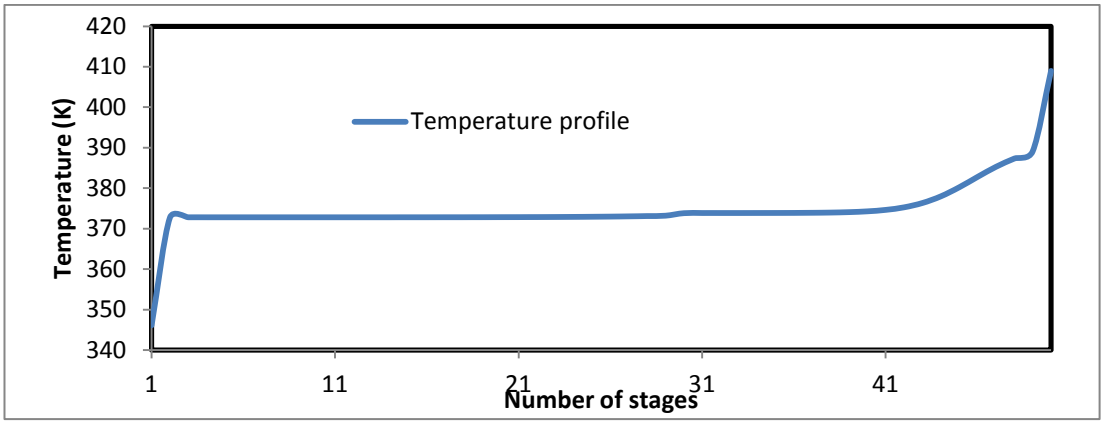

Figure 33: Temperature profile of the 50-stage distillation column.

Table 10 compares the energy demand of the thermal separation units in the three flowsheets simulated. For optimum energy usage, the all the distillation columns were simulated at either twice the minimum number of stage or 1.2 times the minimum reflux ratio. These minimum column variables were determined with the shortcut distillation blocks in Aspen Plus which employs the Winn-Underwood-Gilliland method.

Table 10: Energy usage indicators from the simulated flowsheets.

	SIL scheme Distillation	SIL scheme Flash B4	SIL scheme Flash B6	DIL scheme CASE 1	DIL scheme CASE 2 (water-coolant)	DIL scheme CASE 2
Reboiler temperature (K)	408			445	372	421
Condenser temperature (K)	346	350		307	333	373
Pressure (kPa)	100	100	10	5.33	20	101.3
Condenser duty (kJ/kg IL Feed)	-7749			-4220	-7365	-7066
Reboiler duty (kJ/kg IL Feed)	7848			4372	3640	3661
Reflux ratio	2			1.5	1.5	1.5
Number of stages	50			15	15	15
Flash duty (kJ/kg IL Feed)		-2844	673			

Out of the two different flowsheets simulated with DIL, CASE 1 which effects evaporation of water (antisolvent) without switching-off the DIL require a reboiler duty of about 4372 kJ/kg IL Feed. This scheme results in vacuum operation (5.3 kPa) and 307 K condenser temperature that allows for the usage of water as the coolant. Thus, the cost of cooling can be significantly reduced. The other scheme, CASE 2 that switches-off the DIL yields a reboiler duty of about 3640 and 3661 kJ/kg IL Feed respectively when operated at 20 and 101.3 kPa. The vacuum case can utilize water as the coolant, instead of water the atmospheric case need about 7066 kJ/kg IL Feed of cooling energy at the condenser.

Based on the compared energy-consumption indicators presented in Table 10 for the SIL ([DBUH][$C_4H_9CO_3$]) and DIL ([TMGH][$C_2H_5CO_2$]) in this simulation, it becomes apparent that the DIL is easier and more economical to separate and recycle. The SIL consumes more energy for its components separation partly due to the presence of a gaseous component which requires additional flash tanks and also due to the close-boiling of butanol and water. The boiling point nearness demands 50 stages and 7848 kJ/kg IL Feed reboiler duty to effectively vapourize water from the DBU-butanol. This observation is particularly valuable with regards to selecting antisolvent and or choice of alcohols/organic acids in synthesizing SILs and DILs. However, as noted in King et al. 2011 that lower chain organic acids forms more basic anions which favours biomass dissolution and evaporation. Thus, a trade-off must be made with both observations in order to make a choice that leads to ILs with both adequate biomass dissolution ability and moderate component separation cost.

Lastly, a comparison of flowsheet CASE 1 with the multiflash separation of [emim][OAc] champions the superiority of [emim][OAc]. The trustworthiness of this superiority is; however, dependent on the accuracy of the utilized vapour pressure models. In practice, non-volatile impurities might build-up in the process. This possibility was not considered in these simulations as the nature of such speculated impurities are unknown. Nonetheless, the recycled IL could be boiled-off from such impurities by introducing extra thermal separation units.

6 Discussions and Conclusion

Biomass fractionation with ionic liquids (ILs), on a laboratory scale, has become popular in the literature, mainly with the intent of increasing the capacity and greenness of the bio-based industries. Considering this popularity, different types of ILs—imidazolium-based, TMG-based (DIL) and DBU-based (SIL)—have been reported for their biomass dissolution capability alongside the IL separation and recovery potential. As thermal separation is a common underliner for separating and recycling all this IL types, this thesis seeks to investigate the most promising IL type by modelling and simulating their thermal separation and recycling.

Modelling thermal separation processes naturally demands clear understanding of the vapour-liquid equilibrium (VLE) of the chemical components of interest. In the light of this, the VLE of the ILs-antisolvent mixture for the chosen imidazolium-based IL ([emim][OAc]) was studied. Additionally, the chemical equilibrium (CE) of the chosen DIL ([TMGH][$C_2H_5CO_2$]) and SIL ([DBUH][$C_4H_9CO_3$]) were modelled based on the switchability chemistry assumption. Due to the scarcity of ILs thermodynamics and physical properties data, the models parameter fitting mainly relied on group contribution and other closely applicable estimation methods found in the literature. Furthermore, the CE modelling assumed unity activity coefficients due to lack of experimental data and unavailability of the needed UNIFAC subgroups. Hence, it is noteworthy to acknowledge these weaknesses in the physical properties of the ILs.

Following the VLE and CE modelling, four different biomass fractionation flowsheets were simulated in Aspen Plus with the fitted VLE and CE model parameters appropriately supplied into the simulator. In the simulated flowsheets, the fractionation section was simplified while the thermal separation section was rigorously modelled. Results gathered from the thermal separation conditions of the converged simulations suggest [emim][OAc] to be most energy economic option. In addition, the DIL is more promising than the SIL at least based on the energy spent for the thermal separation. In all the simulations, the antisolvent (water) is mainly being evaporated from the IL/molecular component mixture. This gives credibility to the predicted energy values for the SIL and DIL as their molecular conjugates possess accurate known physical properties. Likewise, the energy values for [emim][OAc] case is trustworthy. However, because the employed saturated vapour pressure of [emim][OAc] is merely an homological value, the credibility of the estimated flash tank pressure will become questionable as the amount of the IL grows.

The energy predictions notwithstanding, it is rather premature to compare the promising potential of the imidazolium-based IL with the switchable ILs (DIL and SIL) due to differences in the model hierarchy (ILs solution chemistry assumptions) and nonideality assumptions. The Gibbs excess (NRTL) model parameters were available for [emim][OAc] while the DIL and SIL assumes ideality both in vapour and liquid phase. Additionally, [emim][OAc] is modelled as a molecular specie while the switchable chemistry is considered for the DIL and SIL.

With regards to the recovery of the spent ILs, an overall statement cannot be given as the dissolution, precipitation and filtration were not rigorously modelled. However, talking about the loss of IL in the thermal section, obviously [emim][OAc] has the highest recovery as it is modelled as a molecular component. On the other hand, the SIL and DIL have to suffer double component loss both in the reactor and in the thermal separation units.

In order to improve these models, several experimental measurements have to be performed. The saturated vapour pressure data for the ILs is important. Likewise, extensive VLE measurement data are important for capturing the nonideality exhibited in the liquid phase. However, considering the cost and time associated with such measurements, the subgroup parameters of UNIFAC method needed for the ILs employed in biomass fractionation could be optimized with the little available measurement data. In addition to that, physical properties prediction with molecular modelling methods could also be engaged in this research area pending the availability of measurement data.

In conclusion, the results from the modelling and simulation of four different biomass fractionation process flowsheets involving three different ILs—[emim][OAc], DIL and SIL—were analyzed to determine the most promising IL. Based on the energy usage of the thermal separation units, the [emim][OAc]-flowsheet is the most promising IL while the DIL-flowsheet consumes less energy as compared to the SIL.

References

Alvarez, V. H.; Saldaña, M. D. A. Thermodynamic prediction of vapor–liquid equilibrium of supercritical CO2 or CHF3 + ionic liquids. *The Journal of Supercritical Fluids* **2012**, *66*, 29-35.

Anderko, A.; Wang, P.; Rafal, M. Electrolyte solutions: from thermodynamic and transport property models to the simulation of industrial processes. *Fluid Phase Equilib.* **2002**, *194–197*, 123-142.

Anugwom, I.; Mäki-Arvela, P.; Virtanen, P.; Willför, S.; Sjöholm, R.; Mikkola, J. -. Selective extraction of hemicelluloses from spruce using switchable ionic liquids. *Carbohydr. Polym.* **2012**, *87*, 2005-2011.

Avami, A.; Saboohi, Y. A simultaneous method for phase identification and equilibrium calculations in reactive mixtures. *Chem. Eng. Res. Design* **2011**, *89*, 1901-1908.

BASF Ionic liquids: Frequently asked questions. http://www.intermediates.basf.com/chemicals/ionic-liquids/faq (accessed March / 01, 2013).

Bedia, J.; Ruiz, E.; de Riva, J.; Ferro, V. R.; Palomar, J.; Rodriguez, J. J. Optimized ionic liquids for toluene absorption. *AIChE J.* **2013**, *59*, 1648-1656.

Bonilla-Petriciolet, A.; Acosta-Martínez, A.; Tapia-Picazo, J. C.; Segovia-Hernández, J. G. A method for flash calculations in reactive mixtures. *Afinidad* **2008**, *65*, 236-242.

Döker, M.; Gmehling, J. Measurement and prediction of vapor-liquid equilibria of ternary systems containing ionic liquids. *Fluid Phase Equilib.* **2005**, *227*, 255-266.

Earle, M. J.; Esperança, J. S. S.; Gilea, M. A.; Canongia Lopes, J. N.; Rebelo, L. P. N.; Magee, J. W.; Seddon, K. R.; Widegren, J. A. The distillation and volatility of ionic liquids. *Nature* **2006**, *439*, 831-834.

Ferro, V. R.; Ruiz, E.; de Riva, J.; Palomar, J. Introducing process simulation in ionic liquids design/selection for separation processes based on operational and economic criteria through the example of their regeneration. *Separation and Purification Technology* **2012**, *97*, 195-204.

Hector, T.; Uhlig, L.; Gmehling, J. Prediction of different thermodynamic properties for systems of alcohols and sulfate-based anion Ionic Liquids using modified UNIFAC. *Fluid Phase Equilib.* **2013**, *338*, 135-140.

Heldebrant, D. J.; Yonker, C. R.; Jessop, P. G.; Phan, L. Organic liquid CO2 capture agents with high gravimetric CO 2 capacity. *Energy and Environmental Science* **2008**, *1*, 487-493.

Hyvarinen, S.; Damlin, P.; Grasvik, J.; Murzin, D. Y.; Mikkola, J. Ionic liquid fractionation of woody biomass for fermentable monosaccharides. *Cellul. Chem. Technol.* **2011**, *45*, 483-486.

Jaime-Leal, J. E.; Bonilla-Petriciolet, A.; Segovia-Hernández, J. G.; Hernández, S.; Hernández-Escoto, H. Analysis and prediction of input multiplicity for the reactive flash separation using reaction-invariant composition variables. *Chem. Eng. Res. Design* **2012**, *90*, 1856-1870.

Jankowski, M. D.; Henry, C. S.; Broadbelt, L. J.; Hatzimanikatis, V. Group contribution method for thermodynamic analysis of complex metabolic networks. *Biophys. J.* **2008**, *95*, 1487-1499.

José M. S. S. Esperança; José, N. C. L.; Mohd Tariq; Luís M. N. B. F. Santos; Joseph W. Magee; Luís, P. N. Volatility of Aprotic Ionic Liquids ◎ A Review. *Journal of Chemical & Engineering Data* **2010**, *55*, 3-12.

Kato, R.; Krummen, M.; Gmehling, J. Measurement and correlation of vapor–liquid equilibria and excess enthalpies of binary systems containing ionic liquids and hydrocarbons. *Fluid Phase Equilib.* **2004**, *224*, 47-54.

Kilpeläinen, I.; Xie, H.; King, A.; Granstrom, M.; Heikkinen, S.; Argyropoulos, D. S. Dissolution of wood in ionic liquids. *J. Agric. Food Chem.* **2007**, *55*, 9142-9148.

King, A. W. T.; Asikkala, J.; Mutikainen, I.; Järvi, P.; Kilpeläinen, I. Distillable acid-base conjugate ionic liquids for cellulose dissolution and processing. *Angewandte Chemie - International Edition* **2011**, *50*, 6301-6305.

Leal, J. P.; Esperança, José M. S. S.; Minas, d. P.; Canongia Lopes, J. N.; Rebelo, L. P. N.; Seddon, K. R. The Nature of Ionic Liquids in the Gas Phase. *J Phys Chem A* **2007**, *111*, 6176-6182.

Lei, Z.; Dai, C.; Liu, X.; Xiao, L.; Chen, B. Extension of the UNIFAC model for ionic liquids. *Industrial and Engineering Chemistry Research* **2012**, *51*, 12135-12144.

Li, B.; Asikkala, J.; Filpponen, I.; Argyropoulos, D. S. Factors affecting wood dissolution and regeneration of ionic liquids. *Industrial and Engineering Chemistry Research* **2010**, *49*, 2477-2484.

Maia, F. M.; Tsivintzelis, I.; Rodriguez, O.; Macedo, E. A.; Kontogeorgis, G. M. Equation of state modelling of systems with ionic liquids: Literature review and application with the Cubic Plus Association (CPA) model. *Fluid Phase Equilib.* **2012**, *332*, 128-143.

Mäki-Arvela, P.; Anugwom, I.; Virtanen, P.; Sjöholm, R.; Mikkola, J. P. Dissolution of lignocellulosic materials and its constituents using ionic liquids—A review. *Industrial Crops and Products* **2010**, *32*, 175-201.

Mavrovouniotis, M. L. Group contributions for estimating standard Gibbs energies of formation of biochemical compounds in aqueous solution. *Biotechnol. Bioeng.* **1990**, *36*, 1070-1082.

Nebig, S.; Gmehling, J. Prediction of phase equilibria and excess properties for systems with ionic liquids using modified UNIFAC: Typical results and present status of the modified UNIFAC matrix for ionic liquids. *Fluid Phase Equilib.* **2011**, *302*, 220-225.

Ober, C. A.; Gupta, R. B. pH Control of Ionic Liquids with Carbon Dioxide and Water: 1-Ethyl-3-methylimidazolium Acetate. *Ind Eng Chem Res* **2012**, *51*, 2524-2530.

Pérez Cisneros, E. S.; Gani, R.; Michelsen, M. L. Reactive separation systems - I. Computation of physical and chemical equilibrium. *Chemical Engineering Science* **1997**, *52*, 527-543.

Poling, B. E.; Prausnitz, J. M.; O'Connell J. P In *Appendix C: Group Contributions for Multiproperty Methods;* The Properties of Gases and Liquids; McGRAW-HILL: 2001; .

Revelli, A.; Mutelet, F.; Jaubert, J. (Vapor + liquid) equilibria of binary mixtures containing light alcohols and ionic liquids. *The Journal of Chemical Thermodynamics* **2010**, *42*, 177-181.

Römich, C.; Merkel, N. C.; Valbonesi, A.; Schaber, K.; Sauer, S.; Schubert, T. J. S. Thermodynamic properties of binary mixtures of water and room-temperature ionic liquids: Vapor pressures, heat capacities, densities, and viscosities of water + 1-ethyl-3-methylimidazolium acetate and water + diethylmethylammonium methane sulfonate. *J. Chem. Eng. Data* **2012**, *57*, 2258-2264.

Safarov, J.; Geppert-Rybczyńska, M.; Hassel, E.; Heintz, A. Vapor pressures and activity coefficients of binary mixtures of 1-ethyl-3-methylimidazolium bis(trifluoromethylsulfonyl)imide with acetonitrile and tetrahydrofuran. *The Journal of Chemical Thermodynamics* **2012**, *47*, 56-61.

Seider, W. D.; Widagdo, S. Multiphase equilibria of reactive systems. *Fluid Phase Equilib.* **1996**, *123*, 283-303.

Smith, J. M.; Van Ness, H. C. *Introduction to Chemical Engineering Thermodynamics;* McGRAW-HILL: New York, 1987; .

Soriano, A. N.; Agapito, A. M.; Lagumbay, L. J. L. I.; Caparanga, A. R.; Li, M. A simple approach to predict molar heat capacity of ionic liquids using group-additivity method. *Journal of the Taiwan Institute of Chemical Engineers* **2010**, *41*, 307-314.

Tan, H. T.; Lee, K. T. Understanding the impact of ionic liquid pretreatment on biomass and enzymatic hydrolysis. *Chem. Eng. J.* **2012**, *183*, 448-458.

Ung, S.; Doherty, M. F. Theory of phase equilibria in multireaction systems. *Chemical Engineering Science* **1995**, *50*, 3201-3216.

Ung, S.; Doherty, M. F. Vapor-liquid phase equilibrium in systems with multiple chemical reactions. *Chemical Engineering Science* **1995**, *50*, 23-48.

Valderrama, J. O.; Rojas, R. E. Critical properties of ionic liquids. Revisited. *Industrial and Engineering Chemistry Research* **2009**, *48*, 6890-6900.

van Spronsen, J.; Cardoso, M. A. T.; Witkamp, G.; de Jong, W.; Kroon, M. C. Separation and recovery of the constituents from lignocellulosic biomass by using ionic liquids and acetic acid as co-solvents for mild hydrolysis. *Chemical Engineering and Processing: Process Intensification* **2011**, *50*, 196-199.

Verevkin, S. P. Predicting enthalpy of vaporization of ionic liquids: A simple rule for a complex property. *Angewandte Chemie - International Edition* **2008**, *47*, 5071-5074.

Wang, P.; Anderko, A. Modeling chemical equilibria, phase behavior, and transport properties in ionic liquid systems. *Fluid Phase Equilib.* **2011**, *302*, 74-82.

Wang, P.; Anderko, A. Modeling chemical equilibria, phase behavior, and transport properties in ionic liquid systems. *Fluid Phase Equilib.* **2011**, *302*, 74-82.

Wei, L.; Li, K.; Ma, Y.; Hou, X. Dissolving lignocellulosic biomass in a 1-butyl-3-methylimidazolium chloride–water mixture. *Industrial Crops and Products* **2012**, *37*, 227-234.

Appendices

APPENDIX A

EQUATION OF STATE MODELS

1. IDEAL GAS

$$pV = nRT \; or \; pv = RT$$

2. Soave-Redlich-Kwong (SRK) model

$$p = \frac{RT}{v-b} - \frac{a\alpha}{v(v+b)}$$

$$a = \frac{0.4274R^2T_c^2}{p_c}$$

$$b = \frac{0.08664RT_c}{p_c}$$

$$\alpha(T) = [1 + (0.48508 + 1.55171\omega - 0.15613\omega^2)(1 - T_r^{0.5})]^2$$

3. Peng-Robinson (PR) CEOS model

$$p = \frac{RT}{v-b} - \frac{a\alpha}{v(v+b)+b(v-b)}$$

4. Virial equation

$$\frac{pv}{RT} = z = 1 + \frac{B}{v} + \frac{C}{v^2}\cdots$$

MIXING RULES

van der Waals mixing rule:

$$a_m = \sum_i \sum_j x_i x_j \sqrt{a_i a_j}(1 - k_{ij})$$

$$b_m = \sum_i \sum_j x_i x_j \sqrt{b_i b_j}(1 - \beta_{ij})$$

The Wong-Sandler mixing rule

$$b_m = \frac{\sum_i \sum_j x_i x_j \left(b - \left({}^{a}/_{RT}\right)\right)_{ij}}{1 - \sum_I \left({}^{x_i a_{ii}}/_{b_{ii} RT}\right) - \left({}^{A_\infty^E}/_{\Omega RT}\right)}$$

$$a_m = b_m \left[\sum_i \frac{x_i a_{ii}}{b_{ii}} + \frac{A_\infty^E}{\Omega}\right]$$

$$\left(b - \left({}^{a}/_{RT}\right)\right)_{ij} = \frac{\left(b_{ii} + b_{jj}\right)}{2} - \frac{\left(1 - k_{ij}\right)\sqrt{a_{ii} a_{jj}}}{RT}$$

$$(a\alpha)_{ij} = \left(1 - k_{ij}\right)\sqrt{(a\alpha)_{ii}(a\alpha)_{jj}}$$

$$a\alpha = \sum \sum y_i y_j (a\alpha)_{ij}$$

$$b = \sum y_i b_i$$

$$k_{ij} = k_{ji}$$

APPENDIX B

VAPOUR PRESSURE MODELS

Antoine equations

$\ln\left(\frac{p}{Pa}\right) = A + \frac{B}{\left(\frac{T}{K}\right)}$ (Two parameters)

$\ln\left(\frac{p}{kPa}\right) = A + \frac{B}{\left(\frac{T}{K}+C\right)}$ (Three parameters)

DIPPR extended form of Antoine

$$\ln\left(\frac{p}{Pa}\right) = A + \frac{B}{\left(\frac{T}{K}\right)} + C\ln\left(\frac{T}{K}\right) + D\left(\frac{T}{K}\right)^{E}$$

E is usually 1, 2 or 6.

Wagner equation

$$\ln\left(\frac{p}{p_c}\right) = (1-x)^{-1}[Ax + Bx^{1.5} + Cx^3 + Dx^6]$$

$$x = 1 - \frac{T}{T_c}$$

Powers of x can also be 1, 1.5, 2.5 and 5.

Cox equation

$$\ln\left(\frac{p}{p(T_b)}\right) = \left(1 - \frac{T_b}{T}\right)\left[A + B\left(\frac{T}{K}\right) + C\left(\frac{T}{K}\right)^2\right]$$

$$p(T_b) = 101.325kPa$$

Frost-Kalkwarf equation

$\ln\left(\frac{p}{Pa}\right) = A + \frac{B}{\left(\frac{T}{K}\right)} + C\ln\left(\frac{T}{K}\right) + D\left(\frac{p/Pa}{T/K}\right)$

APPENDIX C

ACTIVITY COEFFICIENT MODELS

Wilson model

$$\ln \gamma_i = -\ln\left(\sum_j x_j \Lambda_{ji}\right) + 1 - \sum_k \frac{x_k \Lambda_{ki}}{\sum_j x_j \Lambda_{ki}}$$

$$\Lambda_{ji} = \frac{v_j}{v_i} \exp\left(-\frac{\lambda_{ij}}{RT}\right)$$

$$\lambda_{ij} = a_{ij} + b_{ij} T$$

NRTL

$$\frac{G^E}{RT} = \sum_i^N x_i \ln \frac{\sum_j^N G_{ji} \tau_{ji} x_j}{\sum_k^N G_{ki} x_k}$$

$$\tau_{ij} = {U_{ij}}/{RT}$$

$$G_{ij} = \exp\left(-\alpha_{ij} \tau_{ij}\right)$$

$$\alpha_{ij} = \alpha_{ji}$$

Universal Quasi-chemical (UNIQUAC)

$$\ln \gamma_i = \ln {\gamma_i}^C + \ln {\gamma_i}^R$$

$$\ln {\gamma_i}^C = \ln \frac{\Phi_i}{x_i} + \frac{Z}{2} q_i \ln \frac{\theta_i}{\Phi_i} + l_i - \frac{\Phi_i}{x_i} \sum_i x_j l_j$$

$$\ln {\gamma_i}^R = q_i \left[1 - \ln\left(\sum_j \theta_i \tau_{ji}\right) - \sum_j {\theta_j \tau_{ji}}/{\sum_k \theta_k \tau_{kj}}\right]$$

$$\Phi_i = \frac{x_i r_i}{\sum_k x_k r_k}$$

$$\theta_i = \frac{q_i x_i}{\sum_k x_k q_k}$$

$$\tau_{ji} = \exp\left(-\frac{\Delta u_{ij}}{T}\right)$$

$$l_i = \frac{Z}{2}(r_i - q_i) - (r_i - 1)$$

APPENDIX D

SOME EXTIMATED PROPERTIES

[emim][OAc]

Physical properties of [emim][OAc] according to Valderrama and Rojas 2009.

emimOAc critical properties		
	UNIT	
Molecular mass	g/gmol	170.2
Density	kg/m3	1027
Normal boiling point	K	578.8
Critical volume	cm3/mol	544
Critical pressure	bar	29.19
Critical temperature	K	807.1
accentric factor		0.5889
compressibility factor		0.2367

Enthalpy of vapourization at 298 K according to Verevkin 2008

$$\Delta_l^g H_m(\mathrm{IL}) = \sum n_i \Delta H_i + \sum n_j \Delta H_j$$

Table 2: Additivity parameters for calculation of vaporization enthalpies of ILs at 298 K.

Parameter	Value [kJ mol^{-1}]	Parameter	Value [kJ mol^{-1}]
$\Delta H_{(C)}$	2.5	$\Delta H_{(P)}$	4.1
$\Delta H_{(N)}$	26.3	$\Delta H_{(S)}$	−8.2
$\Delta H_{(O)}$	23.6	$\Delta H_{(CF_3)}$	−63.1
$\Delta H_{(B)}$	23.0	$\Delta H_{(ring)}$	27.1
$\Delta H_{(F)}$	13.7		

[emim][OAc] = C8H14N202. Therefore, ΔH_{vap} = 8*2.5 + 2*26.3 + 2*23.6 = 119.8 kJ/mol.

Extrapolated heat capacity from water-[emim][OAc] data reported in Römich et al. 2012 compared with Soriano et al. 2010 additive method prediction.

	T	C_p^L (extrapolated) Römich	C_p^L (predictive) Soriano
UNITS	K	J/(mol-K)	J/(mol-K)
	293.15	310.66	324.06
	303.15	314.33	326.92
	313.15	315.83	330.37
	323.15	319.81	334.42
	333.15	323.72	339.06
	343.15	325.78	344.30
	353.15	330.11	350.13
	363.15	337.58	356.55

The DIL ([TMGH][$C_2H_5CO_2$]) **and SIL** ([DBUH][$C_4H_9CO_3$])

Physical properties calculated based on Valderrama and Rojas 2009.

ILs properties			
		DIL	SIL
	U NIT		
Molecular mass	g/gmol	189	270
Density	kg/m3	1012	764
Normal boiling point	K	541	763
Critical volume	cm3/mol	620	842
Critical pressure	bar	24	14
Critical temperature	K	726	1005
accentric factor		0.7293	0.5400
compressibility factor		0.2441	0.1393

TMG and DBU properties estimated with the Joback method in Flowbat

Property	Dimension	TMG	DBU
MW	g/mol	115.2	152.2
TFREEZ	K	263.1	338.3
TBOIL	K	433.1	533.1
TC	K	624.6	778.1
PC	MPa	3.839	3.736
VC	cm3/mol	368.5	476.5
ZC		0.2724	0.2752
OMEGA		0.5281	0.4558

TMG and DBU ideal gas heat capacity coefficients estimated with the Harris and Seaton's method in Flowbat

Harris and Seaton's property estimation method			
		DBU	TMG
CPA	kJ/mol*K	-0.03483	-0.00458
CPB		0.0009462	0.0006486
CPC		-0.000000572	-3.598E-07
CPD		1.3E-10	7.39E-11

Enthalpy of vapourization data

	FLOWBAT FROM JOBACK		
		DBU	**TMG**
$\Delta H_{vap}(T_b)$	kJ/mol	49.49	33.23
		VEREVKIN 2008	
		DIL	**SIL**
$\Delta H_{vap}(298.15)$	kJ/mol	146.1	158.4

ILs optimized heat capacity coefficients

	SIL	
	J/(mol-K)	
	$C_{p,SIL}^{L}$	$C_{p,SIL}^{IG}$
A	216.97	147.10
B	0.26	0.23
C	0.00	0.00
D	0.00	0.00
E	0.00	0.00

	$C_{p,DIL}$ (J/mol-K)	
	liquid	ideal gas
A	-1063.48	-1196.22
B	4.45	4.80
C	0.00	0.00
D	0.00	0.00
E	0.00	0.00